Revision 2

A new style of rare metal granite with Nb-rich mica: the Early Cretaceous Huangshan rare-metal granite suite, northeast Jiangxi Province, southeast China

ZEYING ZHU[1, 2], RUCHENG WANG[1, *], CHRISTIAN MARIGNAC[2, 3], MICHEL CUNEY[2], JULIEN MERCADIER[2], XUDONG CHE[1], AND MARC-YVES LESPINASSE[2]

[1]State Key Laboratory for Mineral Deposits Research, School of Earth Sciences and Engineering, Nanjing University, Xianlin University Town, Nanjing 210023, China

[2]Université de Lorraine, CNRS, CREGU GeoRessources, Boulevard des Aiguillettes B.P. 70239, F-54506 Vandoeuvre-lès-Nancy, France

[3]Ecole Nationale Supérieure des Mines de Nancy, Parc de Saurupt, F-54042 Nancy, France

* Corresponding author: Ru-Cheng Wang

Address: State Key Laboratory for Mineral Deposits Research, School of Earth Sciences and Engineering, Nanjing University, Xianlin University Town, Nanjing 210023, China

E-mail: rcwang@nju.edu.cn

This is a preprint, the final version is subject to change, of the American Mineralogist (MSA)
Cite as Authors (Year) Title. American Mineralogist, in press.
DOI: https://doi.org/10.2138/am-2018-6511

ABSTRACT

In rare-metal granites, niobium and tantalum are generally hosted by Nb–Ta oxides. However, in SE China, the Nb-specialized Huangshan granites are a unique occurrence in which Nb is essentially hosted by Li–Fe micas. The Huangshan granites are part of the Early Cretaceous (Late Yanshanian) Lingshan granite complex and belong to the A-type granite series, with two facies differing by their mica compositions: medium-grained "protolithionite" granite and medium-grained lithian (lithium-rich) annite granite. The granites are characterized by elevated whole rock Nb contents (average 144 ppm in "protolithionite" granite and 158 ppm in annite granite), quite low Ta contents (average 9 ppm and 4 ppm, respectively), leading to very high Nb/Ta ratios (average 15.3 and 31.2). Niobium is mainly hosted in the micas, with an average Nb content of 1,347 ppm in the lithian annite, and 884 ppm in the "protolithionite", which is the highest ever reported in granitic mica. With an estimated endowment of ~80 kt Nb, the Huangshan granites represent a new style of potential Nb resource. Contrasting with the great rarity of columbite, there is abundant Hf-rich zircon, Y-rich fluorite and Th-rich fluocerite included in the Huangshan micas. Such accessory minerals being typical of alkaline rhyolitic magmas and niobium enrichment in the Huangshan granites results from A-type melt. The extreme Nb enrichment in the micas results from the highly compatible behavior of Nb in this melt, combined with the high magma temperature (estimated at 790–800˚C) and possibly enhanced magma oxidation.

Keywords: Nb-rich mica; Huangshan granite; rare metal; south China

This is a preprint, the final version is subject to change, of the American Mineralogist (MSA)
Cite as Authors (Year) Title. American Mineralogist, in press.
DOI: https://doi.org/10.2138/am-2018-6511

47

48 # INTRODUCTION

49

50 Nb is regarded as a "strategic resource" or a "critical material" by the European
51 Commission (2014) and the U.S. Department of Energy (2011). About 90% of Nb mine
52 production is from pyrochlore and the rest from other oxide minerals such as columbite
53 group minerals (Table 1; Linnen et al. 2014). Consequently, most research and
54 exploration programs have been focused on Nb–Ta oxides (paragenesis, compositional
55 variations, behavior at the magmatic–hydrothermal transition; e.g., Černý and Ercit 1985;
56 Linnen and Keppler 1997; Novák and Černý 1998; Marignac et al. 2001; Linnen and
57 Cuney 2005; Kontak 2006; Van Lichtervelde et al. 2007; Rao et al. 2009; Zhu et al.
58 2015).

59 Micas are one of the key rock-forming minerals in several rock types and are
60 currently used for tracking the magmatic and magmatic–hydrothermal evolution of rare-
61 metal granites (RMG) and pegmatites (e.g., Yashan or Yichun granite, China, Li et al.
62 2015; Tanco pegmatite, Canada, Van Lichtervelde et al. 2008; Cínovec granite, Czech
63 Republic, Johan et al. 2012; Brazil Lake pegmatite, Nova Scotia, Kontak et al. 2006;
64 Karibib pegmatite, Namibia, Roda et al. 2007; Keketuohai region, China, Zhu et al. 2006;
65 Cap de Creus pegmatite field, Spain, Alfonso et al. 2003; Gatuba area pegmatites,
66 Rwanda, Hulsbosch et al. 2014). In addition, mica was proposed to be the major player in
67 fractionation of Nb and Ta within the crust and in magmatic enrichment of Ta (Stepanov
68 and Hermann 2013; Stepanov et al. 2014). However, only a few studies have addressed
69 the trace element concentrations in micas (e.g., Van Lichtervelde et al. 2008; Li et al.

2015; Legros et al. 2016, 2018) and until now they have not been considered as a potential source for economic Nb or Ta.

Southeast China is well endowed with RMGs of different ages and types, and the Yashan (Yichun) and Songshugang RMGs have been particularly well studied (e.g., Yin et al. 1995; Belkasmi et al. 2000; Huang et al. 2002; Zhu et al. 2015). The Huangshan granite/aplite/pegmatite suite (southeast Jiangxi Province, southern China) in the Lingshan plutonic complex displays high Nb and low Ta contents, with some of the highest Nb/Ta ratios reported for RMGs worldwide (Xiang et al. 2017). The granites from this suite contain surprisingly very few Nb–Ta oxides, also in strong contrast to general Nb–Ta-rich RMGs worldwide, and the Nb is almost exclusively concentrated in the micas. Thus the present study aims at providing the first description of the Huangshan RMG, to characterize their Nb-rich and Ta-poor micas and to address the formation conditions of such exceptional mica.

GEOLOGICAL SETTING

Regional setting

The South China Block comprises the Yangtze Block to the northwest and the Cathaysia Block to the southeast (Fig. 1a), which were amalgamated between ca. 1.0 and 0.8 Ga (Tonian) along the 1,500 km NE-trending Jiangnan (or Sibao) orogen (Li et al. 2002, 2009; Mao et al. 2013). With a surface area of 169,700 km^2 comprised of granites and silicic volcanic rocks, the South China Block represents one of the largest granitic

provinces in the world. Nearly 65% of these granites were emplaced during the early (peaking at 160–150 Ma; Jurassic) and the late (ca. 145–65 Ma; Cretaceous) Yanshanian events (Sun 2006; Fig. 1a). The early Yanshanian event has the characteristics of a Silicic Large Igneous Province (SLIP; Xiao et al. 2007; Bryan and Ferrari 2013), and the Yanshanian granites are host rocks for much of the tungsten mined worldwide (Sun et al. 2012).

Tin, tungsten and other rare metals (Nb, Ta, Be and Li) are concentrated in two major belts: the Nanling Range (including three E-W granite belts over a strike length of more than 1,300 km) and the NNE-trending Qin-Hang Belt, along the margin of the former Jiangnan belt (Fig. 1a). The Qin-Hang Belt hosts numerous Cu–Zn–W–Sn–Nb–Ta deposits and contains one of the largest U deposits in China (Mao et al. 2007). The Huangshan complex is located in the northeast of the Qin-Hang Belt, northeastern Jiangxi Province and was emplaced at ca. 130 Ma during the Early Cretaceous (Late Yanshanian) magmatic episode (Zhou et al. 2013; Xiang et al. 2017).

Lingshan complex, host to the Huangshan suite

The Lingshan batholith (~200 km^2) mainly consists of a coarse-grained porphyritic amphibole–biotite granite enriched in microgranular mafic enclaves, rimmed by a coarse-grained biotite granite and intruded by a granite porphyry in the north (Fig. 1b; Zhang and Tian 2005). These intrusions are highly potassic calc-alkaline granites (Xiang et al. 2017). The Huangshan granite suite was emplaced at the boundary between the biotite granite and surrounding hornfels (Cambrian schists). A series of sill-like fine-grained

granites along the same boundary are related to the Huangshan suite (Fig. 1b). A concealed Nb–Ta-rich peraluminous RMG (Songshugang granite) occurs ~3 km west of the Lingshan batholith (Zhu et al. 2015). Reported as the largest Ta reservoir in China (4.2 kt Ta_2O_5), Songshugang suite was emplaced at 124–131 Ma determined by whole-rock K–Ar dating (Zhou et al. 2006), contemporary with the Huangshan suite (ca. 133 Ma; Che et al. 2015) and Lingshan suite (ca. 132 Ma; Xiang et al. 2017). The main body topaz albite granite in Songshugang suite is featured by typical "snow-ball" texture and evident two-stage texture in columbite group minerals and zircons (Zhu et al. 2015). Recent work reveals that beneath Songshugang granite, medium-grained granite similar to Huangshan suite appears. Though the relationship between Huangshan and Songshugang suite is still in dispute, both two suites are generally regarded as part of Lingshan granite pluton (Xiang et al. 2017).

SAMPLING AND ANALYTICAL METHODS

Six samples of medium-grained lithian annite granites (abbreviated as MA granites) were collected from a 50-m-deep drill hole at the top of the Huangshan granite (Fig. 2a) and four samples of medium-grained "protolithionite" granites (abbreviated as MP granite) were collected in a quarry at the bottom of the granite body. Modal compositions were estimated in thin sections using a Keyence VHX-1000 digital optical microscope equipped with image-recognition software. Samples were separated and crushed into 200 μm powders for bulk-rock geochemical analysis. Each sample was at least 15 cm wide and 20 cm long. Major and trace elements were analyzed at the Service d'Analyse des

Roches et des Minéraux (SARM), Centre de Recherches Pétrographiques et Géochimiques (CRPG), Nancy, France. When measuring major element compositions (excluding F and Fe^{III}), the whole-rock powder was mixed with $LiBO_2$, and determined by inductively coupled plasma optical emission spectrometry (ICP-OES, Thermo Fischer ICap 6500). Whole-rock powder was dissolved in acid before obtaining the trace elements including rare earth elements (REE) by inductively coupled plasma mass spectrometry (ICP-MS, Thermo Elemental X7). Fluorine (fusion with Na_2CO_3) and Fe^{III} were determined by potentiometry. Detailed analytical procedures are described in Carignan et al. (2001). The concentrations of all elements (including trace elements) have standard deviations (2δ) of less than 10%.

Quantitative analysis of major element concentrations in micas was first conducted with a JEOL 8100 equipped with four wavelength-dispersive spectrometers (WDS) at the State Key Laboratory for Mineral Deposit Research, School of Earth Sciences and Engineering, Nanjing University, China. The majority of data present in this study were obtained by using a CAMECA SX100 equipped with five WDS spectrometers at GeoRessources Laboratory (Nancy, France). An accelerating voltage of 15 kV and a probe current of 12 nA were used except for Nb (accelerating voltage of 25 kV, probe current of 150 nA). The peak and background counting times were 10 and 5 s, respectively, except for Nb (120 and 60 s), with a beam diameter of 1 μm. The average detection limit for Nb was 90 ppm. TAP (F, Na, Mg, Al, Si, Rb), LPET (K, Cl, Nb), LIF (Mn, Fe), and PET (Cs) crystals were used. Natural and synthetic oxides and silicate standards were used: topaz (F Kα), albite (Na, Si Kα), olivine (Mg Kα), Al_2O_3 (Al Kα), orthoclase (K Kα), vanadinite (Cl Kα), $MnTiO_3$ (Mn, Ti Kα), Fe_2O_3 (Fe Kα), $RbTiPO_5$

(Rb Lα), Cs-pollucite (Cs Lα) and $LiNbO_3$ (Nb Lα). Semi-quantitative X-ray element maps were generated using the electron microprobe under the same operating conditions. Complementary quantitative analysis of zoned micas and other minerals such as zircon, fluorite and REE-F minerals was undertaken in the same laboratory on a JEOL J7600F scanning electron microscope (SEM) equipped with an EDS spectrometer, using the same standards. For accessory minerals, the standards were: monazite (La, Ce, Nd), $REEF_3$ (Gd, Tb, Dy, Ho, Er, Tm, Yb), wollastonite (Ca), $ZrSiO_4$ (Zr, Hf), ThO_2 (Th), UO_2 (U), $LiTaO_3$ (Ta) and $CaWO_4$ (W).

Trace element (Li, Mg, Sc, Ti, Mn, Cs, Rb, Sr, Nb, Ta, W, Sn, Ba, Zr and Hf) concentrations were analyzed by laser inductively coupled mass spectrometry (LA-ICP-MS) for twenty grains of micas from four thin sections (84 spots in total) using aluminium content as an internal standard. A first set of measurements was obtained at the Institute of Geology and Geophysics, Chinese Academy of Sciences, Beijing, China, using an ArF excimer laser ablation system (Geolas CQ) coupled to an Agilent 7500a ICP-MS. The analytical instrument, procedures and detailed operating conditions have been described by Xie et al. (2008). A complementary data set was obtained at the GeoRessources Laboratory in Nancy, using an ArF GeoLas excimer laser ablation system (193 nm, Microlas, Göttingen, Germany, Günther et al. 1997), coupled to an Agilent 7500c ICP-MS. Most spots were located at the same sites of previous EPMA analyses for optimal internal standardization. Analytical conditions were as follows: a fluence of 7 J/cm^2, at a repetition rate of 5 Hz, ablation duration of 40 s, and laser spot sizes of 44, 60, and 90 μm depending on the size of the analyzed mica crystals. To minimize aerosol deposition around the ablation pit, helium (0.5 L/min) was used as a carrier gas to flush

the sample cell during ablation, with argon added prior to injection in the plasma of the mass spectrometer. SRM NIST 610 was used as an external standard and SRM NIST 612 was used to test the analytical reproducibility and accuracy (Jochum et al. 2011). Detection limits for the trace elements were calculated using the Iolite software (Paton et al. 2011).

RESULTS

Geology of the Huangshan suite

The Huangshan granite has not been studied comprehensively since its discovery in 1958 (Liu et al. 2011), and we present observations largely acquired during detailed fieldwork for the present study. The Huangshan suite (Fig. 2a) consists of a granite body (~0.7 km^2) intruded by a series of sill-like pegmatites, fine-grained granites and aplite, which may also extend outside into the hornfels (Fig. 2b). The granite body comprises two homogeneous medium-grained granite sub-units, differing by the composition of micas: lithian annite granite (abbreviated as MA granite) and main "protolithionite" Li-Fe mica (abbreviated as MP granite). A ~100 m-thick layer of MA granite at the top has flat-lying contacts with both the Lingshan biotite granite, and the main MP granite, below the MA granite (Fig. 2b). Owing to the lack of good continuous outcrop, the boundary between the two sub-units was interpolated. The contact could only be observed in a drill hole and appears as transitional over a few centimeters.

The pegmatites consist of quartz and perthitic K-feldspar, with subordinate albite and

rare mica (zinnwaldite), without clear internal zoning. The fine-grained leucogranites are of two types, fine-grained microcline-rich granite and fine-grained albitic granite, only the former being genetically related to the Huangshan granite. Albitic aplite is consistently associated with either the fine-grained albitic granites or the pegmatites, forming banded aplo-pegmatite bodies. Columbite is present in the fine-grained granites and aplite, although it is virtually absent in the pegmatite component. It is on the whole Nb-rich and Mn-poor, whereas Ta-enriched columbite with Ta# [Ta/(Ta + Nb)] up to 0.5 is present in the fine-grained albitic granite and aplite.

Petrography

The medium-grained "protolithionite" (MP) granite comprises 35–40 vol% K-feldspar, 35 vol% quartz, 15 vol% albite, 8–10 vol% "protolithionite" (Fig. 3a–b). Idiomorphic to hypidiomorphic textures are common and the K-feldspar is highly perthitic. The albite lamellae are systematically reorganized into aggregates and bulge into the micas at their boundaries with the K-feldspars, leading to a stellate or cuspate shape of mica (Fig. 3a). In the perthite, the potassic component is almost pure orthoclase and the albite component is also close to the pure end-member (An $\leq$ 0.06). These features indicate a strong subsolidus reorganization of the granitic texture (Bhattacharyya and Sengupta 2014). The MP granite contains a large amount of accessory minerals including zircon, LREE minerals (e.g., parisite, bastnäsite and fluocerite), Y-fluorite and rare columbite (only one crystal observed in all the MP samples). Iron oxides and ilmenite are absent. Except for the widespread argillization of orthoclase in the perthitic

K-feldspar (Fig. 3b), hydrothermal alteration is limited to local chlorite or muscovite development mostly along the rims of "protolithionite". Chloritization and muscovitization are significant only in one sample (15HS02).

The medium-grained lithian annite (MA) granite is quite similar to the MP, the main differences being the composition and texture of the micas. The MA granite contains ~40–45 vol% K-feldspar, 35 vol% quartz, 10 vol% albite and 10 vol% annite, all minerals being subhedral to euhedral. K-feldspar is perthitic and displays similar features as in the MP granite with, however, a less degree of recrystallization. Lithian annite occurs mainly as crystal clusters and display less pronounced cuspate features than in the MP granite (Fig. 3c–d). Argillization of the orthoclase component in perthitic K-feldspar is pervasive (Fig. 3d), whereas chloritization of mica occurs only in one sample (ZK03). Abundant accessory minerals (zircon, Y-fluorite, REE-minerals) and a single columbite grain were observed as inclusions in the mica. Rutile is present in the altered sample (ZK03) associated with chloritization.

Whole-rock geochemistry

The MP granite is characterized by high SiO_2 (75.84–76.25 wt%) and alkali (Na_2O + K_2O = 8.46–8.7 wt%) contents. Calcium (CaO ≤ 0.47 wt%), ferromagnesian (FeOt + MnO + MgO = 2.34–2.64 wt%), and titanium (TiO_2 ≤ 0.07 wt%) concentrations are low. The Fe# [FeOt/(FeOt + MgO)] is close to 1. With ACNK ratios between 0.98 and 1.02 and ANK ratios between 1.04 and 1.06, the MP granite samples lie at the metaluminous–peraluminous boundary, close to the peralkaline field (excluding the altered 15HS02

sample; Fig. 4a; Supplemental Table 1). The MP granites contain significant F (0.32–0.55 wt%) but phosphorus is lower than detection limit. They are enriched in Zr (246–255 ppm) and Hf (12.2–12.7 ppm) with a Zr/Hf ratio of ~20, and high ΣREE (310–424 ppm) and Y (117–142 ppm) concentrations. The bulk-rock Nb content is high (133 to 156 ppm, 144 ppm average) with Ta up to 9.8 ppm. The Nb/Ta ratio ranges from 13.0 to 17.8, with the lower value in the altered 15HS02 sample. Lithium ranges from 346 to 393 ppm, while other rare metals are not significantly concentrated (2.7–3.5 ppm W; 4–4.7 ppm Sn). Finally, the MP granite is Th-rich (72.6–101 ppm) with elevated Th/U ratios, from 2.5 to 16.5 (8.1 in average).

Compared to the MP granite, the MA granite is poorer in calcium ($CaO \leq 0.37$ wt%) but enriched in alkalis (Na_2O+K_2O = 8.58–10.39 wt%), reflecting a slightly higher modal proportion of alkali feldspar. Ferromagnesian concentrations are higher (FeOt + MnO + MgO = 2.4–3.59 wt%), while titanium and phosphorus contents are very low, mostly below detection limit. As in the MP granite, the Fe# is close to 1. The MA granite is poorer in F (0.2–0.43 wt%). ACNK–ANK ratios are close to 1, also at the metaluminous/peraluminous boundary and close to the peralkaline field (ACNK = 0.97–1.03; ANK = 1.02–1.06; Fig. 4a). Compared with the MP granite, the MA granite displays more variable Zr contents (68–428 ppm), poorer in Hf (2.8–14.2 ppm) with higher Zr/Hf ratios (20–30). The ΣREE (278–472 ppm) and Y (78.7–137 ppm) contents are high and comparable to those of the MP granite. The MA granite is equally rich in Nb (112–199 ppm, 158 ppm in average) but poorer in Ta (3.5–6 ppm), yielding high Nb/Ta ratios (22.3–44.9). Lithium is significantly lower than the MP granite (38–177 ppm). Other rare metals are close to Clarke values (W: 2.2–3.5 ppm; Sn: 2.1–4.1 ppm).

277 Compared to the MP granite, Th content is lower (39.3–71.9 ppm) while U content is
278 higher (16.8–24.4 ppm), yielding lower Th/U ratios (2.8–3.1).

279 The Huangshan granites share the characteristics of the evolved "A-type" granites
280 (King et al. 1997), namely: metaluminous to weakly peraluminous, highly silicic (SiO_2 >
281 ~72 wt%), high K_2O + Na_2O and K/Na, high Fe# reflected by the occurrence of Fe-rich
282 mafic minerals (here lithian annite and "protolithionite"), high F (≥ 0.05 wt%) and Cl,
283 high HFSE concentrations (Zr, Hf, REEs and Nb).

284

285 **Accessory mineral inclusion assemblages**

286

287 The numerous accessory minerals are almost included in the micas and rarely occur
288 as interstitial crystals in the groundmass. They were systematically analyzed and imaged
289 by electron microscopy. Representative analyses are present in Supplemental Table 2–3.
290 Inclusions are large (100–200 μm) and unevenly distributed in the micas, from isolated
291 crystals to clusters (up to 10 grains).

292 In the MP granite, the observed assemblages consist of zircon and a complex
293 association of fluorite and REE-minerals in roughly equal proportions (Fig. 5a–b). Zircon
294 is euhedral to subhedral, up to 50 μm wide and 100 μm long. Zircon crystals generally
295 exhibit a patchy zoning with two generations, Zrn-I being overprinted by Zrn-II. Zrn-I is
296 richer in Hf (2.69–6.07 wt% HfO_2) than Zrn-II (2.44 wt% HfO_2), but poorer in U (0.28–
297 0.53 wt% UO_2 in Zrn-I vs. < 1.36 wt% in Zrn-II). In a unique occurrence, small thorite
298 crystals are included in Zrn-I. Fluorite forms round grain, 30 to 80 μm long and 20 to 40
299 μm wide (Fig. 5a–b). Two generations of Y-bearing fluorite are identified: Fl-I is

enriched in Y (5.4–6.30 wt%) and is either rimmed or replaced (patchy zoning) by Y-less Fl-II (Y = 2.59–4.19 wt%). Fluorite-I is typically associated with a fluocerite, enriched in La (11.55–18.4 wt%) and Th (9.31–10 wt%). Fluocerite and Fl-I are intimately associated with exsolution-like textures (Fig. 5c), suggesting that they are coeval (either true exsolution or symplectic association). Fluocerite is commonly observed to be replaced by acicular bastnäsite crystals, related to the recrystallization of Fl-I by Fl-II (Fig. 5c). Two intergrown bastnäsite types are commonly observed, one being Th-rich (Fig. 5b), and thorite crystals may be associated with the bastnäsite. A unique occurrence of a columbite inclusion (100 μm) was found in only one of four representative samples. With a very low Ta# ratio (0.01) and a low Mn# ratio (0.10), it is close to the columbite-(Fe) end-member (Nb/Ta = 76.8). Associated with the alteration of Li–Fe mica to muscovite, small crystals of Nb-rich rutile (Nb_2O_5 up to 9.3 wt%) are observed in a few places (Fig. 5d).

In the MA granite, the primary inclusion assemblages are more variable, including zircon, Y-fluorite + bastnäsite, fluocerite, Y-fluorite + U-pyrochlore and a unique Y-fluorite + columbite-(Fe) + bastnäsite association. As in the MP granite, zircon crystals exhibit a patchy zoning with two generations, displaying the same chemical trends, with higher Hf and less uranium in Zrn-I than in Zrn-II (3.01 wt% HfO_2 in Zrn-I vs. 0.85 wt% in Zrn-II, no U in Zrn-I vs. 0.28 wt% U in Zrn-II), the contents being, however, on the whole lower in the MA granite. As in the MP granite, fluorite is Y-rich and two generations were identified, with Fl-I richer in Y (4.81–6.11 wt%) than Fl-II (1.71–4.48 wt% of Y) and the latter replacing the former. Unlike the MP granite, fluocerite is found as isolated crystals, whereas bastnäsite is commonly associated with the first generation of fluorite or replaces early fluocerite (Fig. 5e). Fluocerite, which is La-rich and Th-

bearing (La = 23.3 wt%; Th = 2.7 wt%) is partially replaced by a La-rich bastnäsite with 2.13 wt% Th, associated with a nearly pure Th-bearing fluocerite rimming the early fluocerite (Fig. 5e). The bastnäsite associated with Fl-I is enriched in Nd relative to La. A rarer assemblage consists of Fl-I hosting small euhedral crystals of a U-rich pyrochlore (Fig. 5f). A unique columbite occurrence was found in one of three representative MA samples (as an aggregate of small prismatic crystals associated with Fl-I + bastnäsite; Fig. 5f). This unzone columbite has a very low Ta# (0.02) and Mn# (0.10) ratio, being a ferrocolumbite (Nb/Ta = 43.3). Aggregates of small rutile crystals are observed in tight association with chlorite along the cleavages of altered lithian annite (Fig. 5h). These rutile grains are Nb-rich, with distinct zoning of Nb_2O_5 from 1.83 to 2.53 wt%. In a unique occurrence, a set of bastnäsite blades (with the same composition as the fluorite-included bastnäsite), associated with thorite crystals, is included in a chlorite matrix (Fig. 5g). This association is suggestive of the pseudomorphing of an earlier mineral. We suggest that this peculiar texture is the result from the dissolution of a fluorite host, replaced by chlorite during mica alteration.

Nb-rich micas

X-ray images and chemical compositions of micas are presented in Supplemental Figure 1 and Table 4–5.

Major element composition and zoning. The mica of the MP granite is homogeneous in BSE, except for some patchy brighter areas up to ~100 μm diameter, appearing in X-ray images which are enriched in Fe. The micas are tri-octahedral, with

346 far more FeO (23.37–26.76 wt%) than MgO (0–0.29 wt%) and MnO (0.29–0.5 wt%).
347 The average TiO_2 concentration is 1.50 wt%. The micas are F-rich (4.29–5.65 wt%) and
348 contain a minor but significant Cl component (~0.17 wt%). In the Al–R^{2+}–Si diagram
349 proposed by Monier and Robert (1986), the MP micas plot on the annite–zinnwaldite–
350 trilithionite tie-line (Fig. 6a), indicating that they are Li-micas. Li_2O was therefore
351 estimated using SiO_2 as a proxy, using the empirical correlations proposed by
352 Tischendorff et al. (1997), yielding Li_2O* between 1.26 and 1.81 wt%. When plotted in
353 the Li–Al–R^{2+} diagram of Foster (1960) (Fig. 6b), the micas are also actually located on
354 the annite–zinnwaldite–trilithionite tie-line, indicating that the lithium was correctly
355 estimated. Thus, the MP mica is classified as a "protolithionite" (Fe–Li mica with an
356 intermediate chemical composition between siderophyllite and zinnwaldite defined by
357 Weiss et al. 1993; Fig. 6c). The structural formula based on the average composition is
358 $(K_{0.98}Rb_{0.03}Na_{0.03})_{1.04}(Fe_{1.71}Mn_{0.03}Mg_{0,02}Li_{0.48}Al^{vi}_{0.51}Ti_{0.09}\square^{vi}_{0.16})(Si_{3.05}Al^{iv}_{0.95}O_{10})(F_{1.32}OH_{0}$
359 $_{.66}Cl_{0.02})_2$.

360 The micas of the MA granite are nearly homogeneous with the exception of sparse
361 variously F- and Fe-rich bands, revealed by BSE and X-ray imagery, possibly
362 representing growth zoning. Compared to the MP "protolithionite", the MA mica is
363 significantly enriched in Fe (FeO = 32.04–34.43 wt%) and Ti (TiO_2 = 1.0–3.2 wt%),
364 while MgO (0.14–0.85 wt%) and MnO (0.21–0.68 wt%) concentrations are low. The F
365 content is lower but still significant (1.92–4.91 wt%) and there is a minor Cl component,
366 slightly higher than MP mica (0.17–0.32 wt%). Following the same procedure as for the
367 MP mica, the MA mica is classified as lithian annite, with an average estimated Li_2O* of
368 0.56 wt% (Fig. 6a–c). The average structural formula is

369 $(K_{0.93}Na_{0.04})_{0.97}(Fe_{2.34}Mn_{0.04}Mg_{0.05}Li_{0.17}Al^{vi}_{0.19}Ti_{0.11}\square^{vi}_{0.27})(Si_{2.96}Al^{iv}_{1.04}O_{10})(F_{1.00}OH_{0.97}Cl_{0.}$

370 $_{03})_2$.

371 **Rare metals and other trace elements.** Micas from the Huangshan MA and MP
372 granites are very rich in Nb (Fig. 7), but low in Ta (19 and 35 ppm in average,
373 respectively), Sn (15 and 31 ppm), and W (1 and 5 ppm; Fig. 8). Niobium contents in
374 micas measured by EPMA and SEM-EDS are consistent with results obtained by LA-
375 ICP-MS (Fig. 7b, d). Most REEs are at concentrations below detection limits in all micas.

376 Lithian annite from the MA granite is the richest in Nb, with concentrations varying
377 from 947 to 1,864 ppm and an average value of 1,348 ppm (LA-ICP-MS), exceptional
378 values up to ~2,900 ppm Nb (EPMA). The brightest BSE domains in the MA mica are
379 slightly depleted in Nb (1,380 ppm) compared to the other domains (1,564–1,864 ppm).
380 "Protolithionite" from the MP granite contains less Nb with less variability: 556 to 1,203
381 ppm, average 884 ppm Nb (LA-ICP-MS); ≤ 1,950 ppm, average 1,170 ppm Nb (SEM-
382 EDS); 970 to 2,900 ppm , average 1,260 ppm Nb (EPMA; Fig. 7a–b). Compared to the
383 MA lithian annite, the MP "protolithionite" is enriched in Ta with a lower Nb/Ta ratio
384 (average 25.5), correlated with a minor increase in Sn (average 31 ppm) and W (average
385 5 ppm; Fig. 8).

386

387 ## DISCUSSION

388

389 ### The Huangshan medium-grained granites as a potential Nb resource

390

391 Huangshan granites contain an average whole-rock Nb content of ~150 ppm,

comparable with some RMGs worldwide, such as Yichun, China (90 ppm; Huang et al. 2002), Orlovka granite, Transbaikalia (145 ppm in the zinnwaldite granite and 255 ppm in the lepidolite granite; Syritso et al. 2001), Kymi stock, Finland (71-229 ppm Nb in the porphyritic granite; Haapala and Lukkari 2005), Beauvoir, France (~150 ppm in the B1 facies; Cuney et al. 1992), and other topaz rhyolites (such as Hideaway park topaz rhyolite, with up to 200 ppm Nb in melt-inclusion of quartz, Mercer et al. 2015; up to 125 ppm Nb in the topaz rhyolites from the Western US, Christiansen et al. 1986). Assuming that the volume of the Huangshan granite body is $\geq \sim 0.2$ km^3 (surface ~ 0.7 km^2, ≥ 300 m thick), the contained Nb amounts is at least ~80 kt ($2.65*0.2*10^9*150*10^{-6}$, assuming a density of 2.65 g/cm^3 for the granite). This resource is comparable to some well-known and major niobium deposits (e.g., Kanyika, Australia, 121 kt Nb; US Geological Survey, 2011).

The peculiarity of the Huangshan granites is that Nb is almost stored by the Fe–Li micas. Considering for example the ZK5 sample (MA granite), the FeO content of the whole-rock is 3.40 wt%, iron being only contained in the micas. Hence the mica amount may be estimated to ~ 10.2% based on the Fe concentrations in lithian annite (33.22 wt% of FeO). Consequently, with an average Nb content of ~ 1,350 ppm (LA-ICP-MS) in lithian annite, this mica contributes in total ~ 138 ppm to the Nb budget of the granite, a value comparable with the 133 ppm Nb measured in the whole-rock. Thus the contribution of other Nb-bearing phases may be considered negligible (including the Nb-rich rutile associate with hydrothermal alteration).

Although the granite body could be easily excavated by open pit mining, and the mica could be separated by flotation, yielding in addition access to the REE-rich

minerals, extraction of Nb from the mica is not economically feasible at present, thus the Huangshan granite body is proposed as a potential niobium resource.

Place of the Huangshan granite among the RMGs

Following Černý and Ercit (2005) and Linnen and Cuney (2005), three main groups of RMGs are recognized: (i) peralkaline rare metal granites and pegmatites (PLK-RMG), including NYF-type [Nb–Y–F], (ii) metaluminous to peraluminous, low-P rare metal granites and pegmatites (PLP-RMG), and (iii) peraluminous intermediate and high-P rare metal granites and pegmatites (IHP- and PHP-RMG), including LCT-type [Li–Cs–Ta]. The Huangshan granites, with their elevated contents in Nb (up to 200 ppm), Zr (up to 300 ppm), ∑REE (up to 500 ppm) and Th (up to 100 ppm), together with rather low Li contents (≤ 370 ppm) and very low Ta/Nb ratios (≤ 0.07), are more akin to the peralkaline RMGs than to the metaluminous to peraluminous, low-P and peraluminous high-P RMGs. However, they are distinctly less enriched in Nb, Zr and REE than the typical peralkaline RMG (up to thousands ppm Nb, up to several weight percent of Zr, and up to 7000 ppm ∑REE; Linnen and Cuney 2005). Such geochemical features are also similar to the other typical A-type RMG-like granites from Arabian Shield (Moghazi et al. 2015) and Erzgebirge, Central Europe (Breiter, 2012).

Importantly, unlike many RMGs worldwide, mica is the primary host for Nb in the Huangshan granitic suite, as demonstrated by the similarity between Ta/Nb ratios in the micas (0.04 for MP and 0.01 for MA granite) and their host rocks (0.07 for MP and 0.04 for MA granites), and by the rarity of other Nb-bearing minerals. Whereas in all other

RMGs Nb is hosted in specific Nb-bearing oxides (mainly pyrochlore in peralkaline RMGs, columbo–tantalite ± microlite in metaluminous to peraluminous, low-P RMGs and peraluminous high-P RMGs). It is therefore worth comparing the Nb concentrations in the Huangshan micas with published contents in micas from rare metal pegmatites (mainly Li-muscovite) and granites (lithian annite to lepidolite) worldwide (Fig. 9; Supplemental Table 6).

The highest Nb content in Li-muscovite (mean = 358 ppm) is reported from the LCT pegmatites in the Cap de Creus area, Spain (Alfonso et al. 2003). Li-muscovite in a pegmatite from the Eastern Brazilian Pegmatite Province has similar Nb contents (204–490 ppm; Viana et al. 2007). Li-muscovite and lepidolite are observed in the Tanco pegmatite (LCT type), with lepidolite containing up to 430 ppm Ta and low Nb (mean = 89 ppm), in accordance with the high Ta/Nb of the rock (Van Lichtervelde et al. 2008). Published muscovite data from other rare metal pegmatite occurrences have lower Nb concentrations, to as low as 21 ppm.

The Fe–Li micas from peralkaline RMGs and metaluminous to peraluminous, low-P RMGs are generally richer in Nb than Li-muscovite when both micas are present in the same complex (Zhu et al. 2006). In the Yashan (Yichun) peraluminous intermediate-P RMG suite, the Nb content is low in all micas, lacking correlation with the degree of fractionation (Li et al. 2015). At Cínovec (Zinnwald), lithian annite from the less fractionated metaluminous to peraluminous, low-P granite contains up to 697 ppm Nb and 269 ppm Ta (Johan et al. 2012). However, in the most fractionated granite, zinnwaldite contains only 124 ppm Nb and 55 ppm Ta. Breiter et al. (2017) also referred medians of 400–800 ppm Nb in annites from Zinnwald and the Nb-content in mica

461 decreases during fractionation. Li-annite from the Nejdek pluton (peraluminous
462 intermediate-P RMG) in western Bohemia displays higher Nb (320 ppm) and Ta (102
463 ppm) contents than micas in other granites (peraluminous high-P or metaluminous to
464 peraluminous, low-P RMGs) from the same province (Fig. 9; Breiter et al. 2017). In the
465 Nechalacho layered peralkaline RMG suite, Canada, Nb concentrations range up to 452
466 ppm in annite (Möller and Williams-Jones 2016).

467 In addition, the Ta/Nb ratios in micas from most RMGs worldwide are higher than
468 the upper continental crust value (Fig. 9), whereas they are lower in the micas from the
469 Huangshan MA and MP granites, emphasizing the exceptional Nb contents in the micas
470 from Huangshan suites.

471

472 **Nb enrichment on the liquid line of descent**

473

474 Unlike columbite, tantalite or other Fe–Ti-rich minerals, few partition coefficients
475 have been determined for Nb in micas within granitic magmas (Linnen and Keppler
476 1997; Horng and Hess 2000; Linnen and Cuney 2005). Experimentally determined Nb
477 partition coefficients between biotite and melt (rhyodacite–rhyolite) at 2.5 to 0.6 GPa and
478 750 to 800˚C are between 0.5 and 9.2 (Nash and Crecraft 1985; Acosta-Vigil et al. 2010;
479 Stepanov and Hermann 2013). These values compare with the empirical ratios of 2.7–5.8
480 obtained by Kovalenko et al. (1977) for the partitioning of Nb between lepidolite and
481 ongonite melt, or the ratio of 3.5 derived by Raimbault and Burnol (1998) for the Nb
482 partition coefficient between Li-muscovite and a Li–F–P-rich rhyolite melt.

483 Stepanov and Hermann (2013) demonstrated the increase of temperature or decrease

of pressure would help increase the Nb partition coefficient between biotite and melt. For the Huangshan granites, we find melt temperatures have been constrained 790–800˚C using the Zr thermometer of Watson and Harrison (1983). Owing to crystal chemistry constraints, the mica–melt Nb partition coefficient also depends on the composition of the mica itself. Johan et al (2012) has proposed three substitution mechanisms in micas:

$$(1)\ 3Ti^{4+} \rightarrow Fe^{2+} + 2(Nb, Ta)^{5+}$$

$$(2)\ 2Ti^{4+} \rightarrow (Fe, Al)^{3+} + (Nb, Ta)^{5+}$$

$$(3)\ 2Al^{3+} \rightarrow Li^{+} + (Nb, Ta)^{5+}$$

In Huangshan micas, substitution (3) is unlikely, given the negative Li–Nb correlation in Fig. 8e, whereas the positive correlation between Fe and Nb (Fig. 8g) is suggestive of the involvement of either (1) or (2) or both. A positive correlation between Ti and Nb is also evident (Fig. 8h). This apparent contradiction may be explained by the observation that Ti in mica is positively correlated with temperature, especially in Fe-rich micas (Robert 1976; Auzanneau et al. 2010): the higher the melt temperature, the higher the Ti content in mica. Therefore, the Nb–Ti correlation is a result of both Nb and Ti being positively correlated with temperature. In view of the Fe^{3+}/Fe^{2+} ratio higher than 1 in the Huangshan MA and MP granites, involvement of substitution (2) is possible and would imply enhanced oxygen fugacity in the Huangshan melt. Yet, a weathering effect could have promoted this high Fe^{3+}/Fe^{2+} ratio, and indeed a strong lateritic event occurred in the Quaternary at the regional scale (Bao and Zhao 2008).

We conclude that the high melt temperatures (~800°C) and possibly the oxidation state of the melt enhanced Nb enrichment in the Huangshan MA and MP granite micas. However, similar conditions are inferred for many other A-type granites where

exceptional Nb enrichment of micas is not observed. Thus, Nb enrichment of the Huangshan micas must also be related to the enrichment of Nb content in the primary Huangshan magmas.

Exceptional Nb enrichment in Huangshan melts

How are Nb-rich melts produced? In peraluminous melts (including the aluminous A-type), Nb–(Ta) oxide saturation is easily reached, and subsequent fractionation generally results in increasing Ta contents (Černý et al. 1986; Xiong et al. 2002; Linnen et al. 2014). It is only in peralkaline silicic melts that enhancement of columbite solubility may allow Nb enrichment through fractionation (Linnen and Cuney 2005). As discussed above, Huangshan granites are more close to the peralkaline field (Fig. 4a).

A key characteristic of both MA and MP granites is the variety and abundance of primary accessory minerals within Nb-rich micas. These early crystallized assemblages are dominated by Hf-bearing zircon, Y-fluorite and REE-fluorides. Hf-bearing zircons and the occurrence of fluorite in place of F-rich topaz are the typical features of peralkaline suites (Wang et al. 2000; Scaillet and Macdonald 2004; Salvi and William-Jones 2005). In the same way, peralkaline silicic melts are enriched in thorium (Linnen and Cuney 2005; Dostal et al. 2014), and Th is abundant in the primary REE-fluorides. As Nb is also typically enriched in peralkaline melts (Salvi and William-Jones 2005), it is therefore most likely that the exceptional Nb content of the Huangshan granites results from this Zr–Y–REE-rich peralkaline melt. In addition, high content of fluorine in the magmatic micas (Fig. 8f) suggest enrichment of fluorine in the original melt, which is

530 also one of the typical features in alkaline magmas. The fluorine in the melt promotes
531 HFSE dissolution through fluoride complexation with Al, thereby making non-bridging
532 oxygen (NBO) available for complexation with the Nb–Ta, or by direct F complexation
533 (Keppler, 1993). In summary, such a melt would have enhanced the solubility of
534 columbite, allowing the incorporation of Nb into the mica and simultaneously explaining
535 the rarity of columbite in the granites.

536 **Origin of the difference between MP and MA granites.** From lithian annite in
537 MA granites to "protolithionite" in MP granites, Ta content increases from 18.7 to 35.7
538 ppm, correlated with a decrease in both Nb concentration (1,348–884 ppm) and Nb/Ta
539 ratio (72.1–25.5; Fig. 8). These variations are consistent with fractional crystallization,
540 with the MP granite representing the more evolved member of the suite. Micas from early
541 less fractionated facies of Huangshan MA are Li-poorer, but more Nb-enriched than
542 micas from the late, more fractionated facies (MP). The possible interpretation is that Li-
543 annite is an early mineral in less fractionated RMG sequestering a big portion of available
544 Nb into its lattice. In Li and F-rich late facies, the crystallization of Nb-rich mica
545 contributes to consuming Nb in the melt, resulting in the later crystallization of Nb-poor
546 mica. The increase in fluorine contents may contribute to the extreme fractionation,
547 leading to an increase of Ta in the residual melt and crystallization of the relatively Ta-
548 rich "protolithionite".

549

550 **Post-magmatic events and their effects on Nb concentrations**

551

552 Magmatic textures in the Huangshan granites were reworked, resulting in

553 recrystallization of perthitic K-feldspar, patchy zoning in zircon, the Fl-I to Fl-II
554 transition, and the transformation of fluocerite into bastnäsite, all occurring without
555 perceptible alteration of the hosting mica. These processes are therefore inferred to have
556 occurred at high temperature, either at the end of magma crystallization or just below the
557 solidus, meaning that they are most likely the product of interaction with magmatic fluids
558 (i.e., fluids released from the residual melt at the magmatic–hydrothermal transition). In
559 the MP granite, "protolithionite" contains Fe-rich patchy areas, which likely result from
560 high temperature fluid–rock interaction, also possible at the magmatic–hydrothermal
561 transition. Whatever the timing, the Fe-rich areas are weakly Nb-depleted (766 ppm)
562 indicating a small amount of Nb could have been lost during this interaction.

563 The common replacement of fluocerite by bastnäsite crystals, spatially related to the
564 replacement of Fl-I by Fl-II with loss of Y, is consistent with the data on mineral-fluid
565 equilibria at 300°C and 400°C for the stability of bastnäsite-(Ce)-, parisite-(Ce)- and
566 fluocerite-(Ce)-bearing mineral assemblages as a function of dissolved ion activities (aF^-
567 and aCO_3^{2-}; Gysi and Williams-Jones 2015), and could therefore be also a subsolidus
568 process.

569 When the Fe–Li micas were altered to chlorite or muscovite, we infer that the
570 released niobium was partitioned into rutile (Fig. 5d, h), leading to the formation of Nb-
571 rich rim. However, it is in the most altered sample (15HS02) that the Nb/Ta ratio is the
572 lowest (Fig. 4b); therefore suggesting that a limited amount of Nb was lost during the
573 hydrothermal alteration.

574

575 **IMPLICATIONS**

With an average content of ~150 ppm Nb (158 ppm in the lithian annite granite, 144 ppm in the "protolithionite" granite), the Huangshan granite suite is Nb-mica-specialized. The Huangshan granites are characterized by the highest Nb contents measured to date in micas from granites, with an average 1,347 ppm in the lithian annite and 884 ppm in the "protolithionite". These Nb-rich micas are the main contributors to the Nb budget in the hosting granites, with very rare primary columbite or Nb-rutile associated with hydrothermal alteration contributing negligible amounts. In this respect, the Huangshan granites are at present unique among the rare metal granites worldwide. With an estimated ~80 kt of contained Nb, the Huangshan complex represents a new class of Nb resource, the development of which awaits advancement of a feasible economic extraction process to separate Nb from the micas.

The Huangshan granites are of the A-type granites. The abundant primary mineral inclusions in the micas (Hf-rich zircon, Y-rich fluorite, and Th-rich fluocerite), point to a peralkaline affinity. The extreme Nb enrichment in Huangshan micas is also due to the strong solubility of columbite in the magma, allowing high Nb mica–melt partition coefficients, enhanced by high temperature and possibly high oxidation state in the magma.

ACKNOWLEDGMENTS

We thank Andrei Lecomte, Sandrine Mathieu, Chantal Peiffert and Olivier Rouer for their help during data acquisition at the GeoRessources Laboratory Nancy, France; Wen-

599 Lan Zhang and Juan Li for their assistance at the State Key Laboratory for Mineral
600 Deposits, Nanjing University; and Yue-Heng Yang for his help at the Institute of
601 Geology and Geophysics, Chinese Academy of Sciences, Beijing, China. Karel Breiter,
602 Aleksandr Stepanov, and Associate Editor Celeste Mercer are sincerely thanked for their
603 detailed and helpful review to improve the manuscript. Roger Skirrow (Geoscience
604 Australia) and an anonymous English native speaker are warmly thanked for improving
605 the language.

606 This study was supported by the National Key R&D Project of China
607 (2016YFC0600203), the Natural Science Foundation of China (Grant 41230315 and
608 41672065). This study forms part of Ze-Ying Zhu's doctoral thesis at the Nanjing
609 University (China) and at the Université de Lorraine (France), supported by the
610 Caiyuanpei program from China Scholarship Council (CSC).

611

612 **REFERENCES**

613

614 Acosta-Vigil, A., Buick, I., Hermann, J., Cesare, B., Rubatto, D., London, D., and
615 Morgan, VI. GB. (2010) Mechanisms of crustal anatexis: a grochemical study of
616 partially melted metapelitic enclaves and host Dacite, SE Spain. Journal of Petrology,
617 51, 785–821.

618 Alfonso, P., Melgarejo, J.C., Yusta, I., and Velasco, F. (2003) Geochemistry of feldspars
619 and muscovite in granitic pegmatite from the Cap de Creus field, Catalonia, Spain.
620 The Canadian Mineralogist, 41, 103–116.

621 Auzanneau, E., Schmidt, M.W., Vielzeuf, D., and D Connolly, J.A. (2010) Titanium in

622 phengite: a geobarometer for high temperature eclogites. Contributions to
623 Mineralogy and Petrology, 159, 1–24.
624 Bao, Z.W., and Zhao, Z.H. (2008) Geochemistry of mineralization with exchangeable
625 REEY in the weathering crust of granitic rocks in South China. Ore Geology
626 Reviews, 33, 519–535.
627 Belkasmi, M., Cuney, M., Pollard, P.J., and Bastoul, A. (2000) Chemistry of the Ta–Nb–
628 Sn–W oxide minerals from the Yichun rare metal granite (SE China): genetic
629 implications and comparison with Moroccan and French Hercynian examples.
630 Mineralogical Magazine, 64, 507–523.
631 Bhattacharyya, S., and Sengupta, S. (2014) Modelling of dissolution-reprecipitation ion–
632 exchange reactions for the development of flame perthite in suite of sheared alkaline
633 rocks: an example from Chinmakurthy, Eastern Ghats, India. Mineralogical
634 Magazine, 78, 1301–1323.
635 Breiter K. (2012) Nearly contemporaneous evolution of the A- and S-type fractionated
636 granites in the Krušné hory/Erzgebirge Mts., Central Europe. Lithos, 152, 105–121.
637 Breiter, K., Vaňková, M., Galivá Vašinová, M., Korbelová, Z. and Kanický, V. (2017)
638 Lithium and trace-element concentrations in trioctahedral micas from granites of
639 different geochemical types measured via laser ablation ICP-MS. Mineralogical
640 Magazine, 81, 15–33.
641 British Geological Survey (2011) Niobium–tantalum [Online]. Available:
642 https://www.bgs.ac.uk/downloads/start.cfm?id =2033 [accessed 2018 January 4].
643 Bryan, S.E., and Ferrair, L. (2013) Large igneous provinces and silicic large igneous
644 provinces; progress in our understanding over the last 25 years. Geological Society of

America Bulletin, 125, 1053–1078.

Carignan, J., Hild, P., Mevelle, G., Morel, J., and Yeghicheyan, D. (2001) Routine analysis of trace elements in geological samples using flow injection and low pressure on–line liquid chromatography coupled to ICP–MS: a study of geochemical reference materials BR, DR–N, UB–N, AN–G and GH. Geostandards Newsletter, 25, 187–198.

Černý, P., and Ercit, T.S. (1985) Some recent advances in the mineralogy and geochemistry of Nb and Ta in rare–element granitic pegmatites. Bulletin de Minéralogie, 108, 499–532.

Černý, P., Goad, B.E., Hawthornw, F.C., and Chapman, R. (1986) Fractionation trends of the Nb- and Ta-bearing oxide minerals in the Greer Lake pegmatitic granite and its pegmatite aureole, Southeastern Manitoba. American Mineralogist, 71, 501–517.

Černý, P., and Ercit, T.S. (2005) The classification of granitic pegmatites revised. The Canadian Mineralogist, 43, 2005–2026.

Che, X.D., Wu, F.Y., Wang, R.C., Gerdes, A., Ji, W.Q., Zhao, Z.H., Yang, J.H., and Zhu, Z.Y. (2015) In situ U–Pb isotopic dating of columbite–tantalite by LA–ICP–MS. Ore Geology Reviews, 85, 979–989.

Christiansen, E.H., Sheridan, M.F., and Burt, D.M. (1986) The geology and geochemistry of Cenozoic topaz rhyolites from the Western United States. In Geological Society of America. pp. 1–82.

Cuney M, Marignac C, and Weisbrod A (1992) The Beauvoir topaz-lepidolite albite granite (Massif Central, France): the disseminated magmatic Sn–Li–Ta–Nb–Be mineralization. Economic Geology, 87, 1766–1794.

668 Dostal, J., Kontak, D.J, and Karl, S.M. (2014) The early Jurassic Bokan Mountain
669 peralkaline granitic complex (southeastern Alaska): geochemistry, petrogenesis and
670 rare-metal mineralization. Lithos, 202–203, 395–412.
671 European Commission (2014) Report on critical raw material for the EU [Online].
672 Available: http://www.catalysiscluster.eu/wp/wp-
673 content/uploads/2015/05/2014_Critical-raw-materials-for-the-EU-2014.pdf [accessed
674 2017 March 10].
675 Foster, M.D. (1960) Interpretation of the composition of trioctahedral micas. U.S.
676 Geological Survey Professional Paper, 354-E, 115–147.
677 Günther, D., Frischknecht, R., Heinrich, C.A., and Kahlert, H.J. (1997) Capabilities of an
678 argon fluoride 193 nm excimer laser for laser ablation inductively coupled plasma
679 mass spectrometry microanalysis of geological materials. Journal of Analytical
680 Atomic Spectrometry, 12, 939–944.
681 Gysi, A., and Williams-Jones, A.E. (2015) The thermodynamic properties of bastnäsite-
682 (Ce) and parisite-(Ce). Chemical Geology, 392, 87–101.
683 Haapala, I., and Lukkari, S. (2005) Petrological and geochemical evolution of the Kymi
684 stock, a topaz granite cupola within the Wiborg rapakivi batholith, Finland. Lithos,
685 80, 347–362.
686 Horng, W.S., and Hess, P.C. (2000) Partition coefficients of Nb and Ta between rutile and
687 anhydrous haplogranite melts. Contributions to Mineralogy and Petrology, 138, 176–
688 185.
689 Huang, X.L., Wang, R.C., Chen, X.M., Hu, H., and Liu, C.S. (2002) Vertical variations in
690 the mineralogy of the Yichun topaz–lepidolite granite, Jiangxi Province, southern

691 China. The Canadian Mineralogist, 40, 1047–1068.
692 Hulsbosch, N., Hertogen, J., Dewaele, S., André, L., and Muchez, P. (2014) Alkali metal
693 and rare earth element evolution of rock–forming minerals from the Gatumba area
694 pegmatites (Rwanda): Quantitative assessment of crystal–melt fractionation in the
695 regional zonation of pegmatite groups. Geochimica et Cosmochimica Acta, 132,
696 349–374.
697 Jochum, K.P., Weis, U., Stoll, B., Kuzmin, D., Yang, Q., Raczek, I., Jacob, D.E., Stracke,
698 A., Birbaum, K., Frick, D.A., Gunther, D., and Enzweiler, J. (2011) Determination of
699 reference values for NIST SRM 610–617 glasses following ISO guidelines.
700 Geostandards and Geoanalytical Research, 35, 397–429.
701 Johan, Z., Strnad, L., and Johan, V. (2012) Evolution of the Cínovec (Zinnwald) granite
702 cupola: Czech Republic: composition of feldspars and micas, a clue to the origin of
703 W, Sn mineralization. The Canadian Mineralogist, 50, 1131–1148.
704 King, P.L., White, A.J.R., Chappell, B.W., and Allen, C.M. (1997) Characterization and
705 origin of aluminous A–type granites from the Lachlan Fold Belt, southeastern
706 Australia. Journal of Petrology, 38, 371–391.
707 Kontak, D.J. (2006) Nature and origin of an LCT-suite pegmatite with late–stage sodium
708 enrichment, Brazil Lake, Yarmouth County, Nova Scotia. I. Generogical setting and
709 petrology. The Canadian Mineralogist, 44, 563–598.
710 Kovalenko, VI., Antipin, V.S., Konusova, V.V., Smirnova, YeV., Petrov, L.L., Vladykin,
711 N.V., Kuznetsova, AI., Kostyukova, YeS., and Pisarskaya, V.A. (1977) Partition
712 coefficients of fluorine, niobium, tantalum, lanthanum, ytterbium, yttrium, tin and
713 tungsten in ongonite. Doklady Earth Science, 233, 203–205.

714 Legros, H., Marignac, C., Mercadier, J., Cuney, M., Richard, A., Wang, R.C., Charles, N,
715 and Lespinasse, M.Y. (2016) Detailed paragenesis and Li-mica compositions as
716 recorders of the magmatic–hydrothermal evolution of the Maoping W–Sn deposit
717 (Jiangxi, China). Lithos, 264, 108–124.
718 Legros, H., Marignac, C., Tabary, T., Mercadier, J., Richard, A., Cuney, M., Wang R.C.,
719 Charles, N., and Lespinasse, M.Y. (2018) The ore-forming magmatic–hydrothermal
720 system of the Piaotang W–Sn deposit (Jiangxi, China) as seen from Li-mica
721 geochemisty. American Mineralogist, 103, 39–54.
722 Li, J., Huang, X.L., He, P.L., Li, W.X., Yu, Y., and Chen, L.L. (2015) In situ analyses of
723 micas in the Yanshan granite, South China: Constraints on magmatic and
724 hydrothermal evolutions of W and Ta–Nb bearing granites. Ore Geology Reviews,
725 65, 793–810.
726 Li, X.H., Li, W.X., Li, Z.X., Lo, C.H., Wang, J., Ye, M.F., and Yang, Y.H. (2009)
727 Amalgamation between the Yangtze and Cathaysia Block in South China: Constraints
728 from SHRIMP U–Pb zircon ages, geochemistry and Nd–Hf isotopes of the
729 Shuangxiwu volcanic rocks. Precambrian Research, 174, 117–128.
730 Li, Z.X., Li, X.H., Zhou, H.W., and Kinny, P.D. (2002) Grenvillian continental collision
731 in south China: new SHRIMP U–Pb zircon results and implications for the
732 configuration of Rodinia. Geology, 30, 163–166.
733 Linnen, R.L., and Keppler, H. (1997) Columbite solubility in granitic melts:
734 consequences for the enrichment Novák and fractionation of Nb and Ta in the Earth's
735 crust. Contributions to Mineralogy and Petrology, 128, 213–227.
736 Linnen, R.L., and Cuney, M. (2005) Granite-related rare-element deposits and

737 experimental constraints on Ta–Nb–W–Sn–Zr–Hf mineralization. In R.L. Linnen and
738 I.M. Samson Eds., Rare-Element Geochemistry and Mineral Deposits GAC Short
739 Course Notes, 17, p. 45–67. Geological Association of Canada.
740 Linnen, R.L., Samson, I.M., Williams–Jones, A.E., and Chakhmouradian, A.R. (2014)
741 Geochemistry of the rare-earth element, Nb, Ta, Hf, and Zr deposits. In H. Heinrich
742 and T. Karl, Eds., Reference Module in Earth Systems and Environmental Sciences
743 Treatise on Geochemistry, p. 543–564. Elsevier Science.
744 Liu, Y.H., Li, K.Y., and Tu, J.F. (2011) Geological characteristics and genesis of
745 Huangshan niobium (tantalum) deposit in Geyuan, Jiangxi Province. Resources
746 Survey & Environment, 4, 291–298 (in Chinese with English abstract).
747 Mao, J.W., Xie, G.Q., Guo, C.L., and Chen, Y.C. (2007) Large–scale tungsten–tin
748 mineralization in the Nanling region, South China: Metallogenic ages and
749 corresponding geodynamic processes. Acta Petrologica Sinica, 23, 2329–2338 (in
750 Chinese with English abstract).
751 Mao, J.W., Cheng, Y.B., Cheng, M.H., and Pirajno, F. (2013) Major types and time-space
752 distribution of Mesozoic ore deposits in South China and their geodynamic settings.
753 Mineralium Deposita, 48, 267–294.
754 Marignac, C., Belkasmi, M., Chalal, Y., and Kesraoui, M. (2001) W–Nb–Ta oxides as
755 markers of the magmatic to hydrothermal transition condition in rare–metal granites.
756 In A. Piestrzynski, Eds., Mineral deposits at the beginning of the 21st century, p.
757 441–444. Biennial SGA Meeting, Krakow, Poland, Balkema, Rotterdam.
758 Mercer, C.N., Hofstra, A.H., Tordorov, T.I., Roberge, J., Burgisser, A., Adams, D.T., and
759 Cosca, M. (2015) Pre-eruptive conditions of the Hideaway Park topaz rhyolite:

760 insights into metal source and evolution of magma parental to the Henderson
761 porphyry molybdenum deposit, Colorado. Journal of Petrology, 56, 645–679.
762 Möller, V., and Williams–Jones, A.E. (2016) Petrogenesis of the Nechalacho layered
763 suite, Canada: magmatic evolution of a REE–Nb-rich nepheline syenite intrusion.
764 Journal of Petrology, 57, 229–276.
765 Moghazi, A.M., Iaccheri, L.M., Bakhsh, R.A., Kotov, A.B., and Ali, K.A. (2015) Sources
766 of rare-metal-bearing A-type granites from Jabel Sayed complex, Northern Arabian
767 Shield, Saudi Arabia. Journal of Asian Earth Sciences, 107, 244–258.
768 Monier, G., and Robert, J.L. (1986) Evolution of the miscibility gap between muscovite
769 and biotite solid solutions with increasing lithium content: an experimental study in
770 the system K_2O–Li_2O–MgO–FeO–Al_2O_3–SiO_2–H_2O–HF at 600°C, 2 kbar PH_2O:
771 comparison with natural lithium micas. Mineralogical Magazine, 50, 641–651.
772 Nash, W.P., and Crecraft, H.R. (1985) Partition coefficients for trace elements in silicic
773 magmas. Geochimica et Cosmochimica Acta, 49, 2309–2322.
774 Novák, M., and Černý, P. (1998) Niobium–tantalum oxide minerals from complex
775 granitic pegmatites in the moldanubicum, Czech Republic: primary versus secondary
776 compositional trends. The Canadian Mineralogist, 36, 659–672.
777 Paton, C., Hellstrom, J., Paul, B., Woodhead, J., and Hergt, J. (2011) Iolite: freeware for
778 the visualization and processing of mass spectrometric data. Journal of Analytical
779 Atomic Spectometry, 26, 2508.
780 Raimbault, L., and Burnol, L. (1998) The Richemont rhyolite dyke, Massif Central,
781 France: a subvolcanic equivalent of rare-metal granites. The Canadian Mineralogist,
782 36, 265–282.

783 Rao, C., Wang, R.C., Hu, H., and Zhang, W.L. (2009) Complex internal textures in oxide
784 minerals from the Nanping No. 31 dyke of granitic pegmatite, Fujian Province,
785 southeastern China. The Canadian Mineralogist, 47, 1195–1212.
786 Robert, J.L. (1976) Phlogopite solid solutions in the system K_2O–MgO–Al_2O_3–SiO_2–
787 H_2O. Chemical Geology, 17, 195–212.
788 Roda, E., Keller, P., Pesquera, A., and Fontan, F. (2007) Micas of the muscovite–
789 lepidolite series from Karibib pegmatites, Namibia. Mineralogical Magazine, 71(1),
790 41–62.
791 Rudnick, R., and Gao, S. (2003) Composition of the continental crust. Treatise on
792 Geochemistry, 3, 1–64.
793 Salvi, S., and Williams–Jones, A.E. (2005) Alkaline granite-syenite hosted deposits. In:
794 R.L. Linnen, and I.M. Samson, Eds., Rare-Element Geochemistry and Mineral
795 Deposits, 17, p. 315–341. Short Course Notes-Geological Association of Canada.
796 Scaillet, B., and Macdonald, R. (2004) Fluorite stability in silicic magmas. Contributions
797 to Mineralogy and Petrology, 147, 319–329.
798 Stepanov, A., and Hermann, J. (2013) Fractionation of Nb and Ta by biotite and phengite:
799 implication for the “missing Nb paradox”. Geology, 41, 303–306.
800 Stepanov, A., Mavrogenes, J.A., Meffre, S., and Davidson, P. (2014) The key role of mica
801 during igneous concentration of tantalum. Contribution to Mineralogy and Petrology,
802 167, 1009.
803 Sun, T. (2006) A new map showing the distribution of granites in South China and its
804 explanatory notes. Geological Bulletin of China, 25, 332–335 (in Chinese with
805 English abstract).

Sun, W.D., Yang, X.Y., Fan, W.M., and Wu, F.Y. (2012) Mesozoic large scale magmatism and mineralization in South China: Preface. Lithos, 150, 1–5.

Syritso, L.F., Tabuns, E.V., Volkova, E.V., Badanina, E.V., and Vysotskii, Y.A. (2001) Model for the genesis of Li-F granites in the Orlovka Massif, eastern Transbaikalia. Petrology, 9, 268–289.

Teng, F.Z., McDonough, W.F., Rudnick, R.L., Dalpé, C., Tomascak, P.B., Chappell, B.W., and Gao, S. (2004) Lithium isotopic composition and concentration of the upper continental crust. Geochimica et Cosmochimica Acta, 68, 4167–4178.

Tischendorff, G., Gottesmann, B., Förster, H.J., and Trumbull, R.B. (1997) On Li–bearing micas: estimating Li from electron microprobe analyses and an improved diagram for graphical representation. Mineralogical Magazine, 61, 809–834.

U.S. Department of Energy (2011) Critical Materials Strategy [Online]. Available: https://energy.gov/sites/prod/files/DOE_CMS2011_FINAL_Full.pdf. [accessed 2017 November 22]

U.S. Geological Survey (2011) Minerals Yearbook Niobium and tantalum (Advance Release) [Online]. Available: https://minerals.usgs.gov/minerals/pubs/commodity/niobium/myb1-2011-niobi.pdf [accessed 2018 January 4]

Van Lichtervelde, M., Salvi, S., Béziat, D., and Linnen, R.L. (2007) Textural features and chemical evolution in tantalum oxides: magmatic versus hydrothermal origins for Ta mineralization in the Tanco lower pegmatite, Manitoba, Canada. Economic Geology, 102, 257–276.

Van Lichtervelde, M., Grégoire, M., Linnen, R.L., Béziat, D., and Salvi, S. (2008) Trace

element geochemistry by laser ablation ICP-MS of micas associated with Ta mineralization in the Tanco pegmatite, Manitoba, Canada. Contributions to Mineralogy and Petrology, 155, 791–806.

Viana, R.R., Jordt-evangelista, H., and Stern, W.B. (2007) Geochemistry of muscovite from pegmatites of the Eastern Brazilian pegmatite province: a clue to petrogenesie and mineralization potential. European Journal of Mineral Chemistry, 19, 745–755.

Wang, R.C., Zhao, G.T., Lu, J.J., Chen, X.M., Xu, S.J., and Wang, D.Z. (2000) Chemistry of Hf–rich zircons from the Laoshan I- and A-type granites, Eastern China. Mineralogical Magazine, 64, 867–877.

Watson, E.B., and Harrison, T.M. (1983) Zircon saturation revisited: temperature and composition effects in a variety of crustal magma types. Earth and Planetary Science Letters, 64, 295–304.

Weiss, Z., Rieder, M., Smrcok, L., Vaclav, P., and Bailey, S.W. (1993) Refinement of the crystal structures of two “protolithionite”. European Journal of Mineralogy, 5, 493–502.

Xiang, Y.X., Yang, J.H., Chen, J.Y., and Zhang, Y. (2017) Petrogenesis of Lingshan highly fractionated granites in the Southeast China: Implication for Nb–Ta mineralization. Ore Geology Reviews, 89, 497–525.

Xiao, L., Pirajno, F., and He, Q. (2007) A preliminary discussion on large igneous provinces and associated ore deposits. Geological Journal of China Universities, 13, 148–160 (in Chinese with English abstract).

Xie, L.W., Zhang, Y.B., Zhang, H.H., Sun, J.F., and Wu, F.Y. (2008) In situ simultaneous determination of trace elements, U–Pb and Lu–Hf isotopes in zircon and baddeleyite.

852 Chinese Science Bulletin, 53, 1565–1573.

853 Xiong, X.L., Rao, B., Chen, F.R., Zhu, J.C., and Zhao, Z.H. (2002) Crystallization and
854 melting experiments of a fluorine-rich leucogranite from the Xianghualing Pluton,
855 South China, at 150 MPa and H_2O-saturated conditions. Journal of Asian Earth
856 Sciences, 21, 175–188.

857 Yin, L., Pollard, P.J., Hu, S.X., and Taylor, R.G. (1995) Geologic and geochemical
858 characteristics of the Yichun Ta–Nb–Li deposit, Jiangxi Province, South China.
859 Economic Geology, 90, 577–585.

860 Zhang, P., and Tian, B. (2005) Primary discussion on the characteristics and
861 metallogenesis of Lingshan composite massif in northeastern Jiangxi Province. World
862 Nuclear Geoscience, 1, 31–38 (in Chinese with English abstract).

863 Zhou, J., Jiang, Y.H., Xing, G.F., Zeng, Y., and Ge, W.Y. (2013) Geochronology and
864 petrogenesis of Cretaceous A-type granites from the NE Jiangnan Orogen, SE China.
865 International Geology Review, 55, 1359–1383.

866 Zhu, Y.F., Zeng, Y.S., and Gu, L.B. (2006) Geochemistry of the rare metal–bearing
867 pegmatite No. 3 vein and related granites in the Keketuohai region, Altay Mountains,
868 northwest China. Journal of Asian Earth Sciences, 27, 61–77.

869 Zhu, Z.Y., Wang, R.C., Che, X.D., Zhu, J.C., Wei, X.L., and Huang, X.E. (2015)
870 Magmatic–hydrothermal rare-element mineralization in the Songshugang granite
871 (northeastern Jiangxi, China): insights from an electron–microprobe study of Nb–Ta–
872 Zr minerals. Ore Geology Reviews, 65, 749–760.

873

874 **Figure captions**

875

876 **Figure 1.** (a) The granite province of SE China, with location of the Nanling Range and
877 Qin-Hang belt and the main rare-metal (Nb–Ta–W–Sn) deposits (modified after Sun
878 2006 and Li et al. 2015). (b) The Lingshan granite complex (modified after Zhang and
879 Tian, 2005).

880

881 **Figure 2.** (a) Geological map of the Huangshan granite suite (modified after Liu et al.
882 2011); (b) Schematic cross-section (general location in Fig.2a).

883

884 **Figure 3.** The two Huangshan granite facies: (a-b) medium-grained "protolithionite"
885 granite (MP granite); note the cuspate mica shape in relation with the reorganization of
886 the perthite lamellae. (c-d) medium-grained annite granite (MA granite). Qz = quartz; Kfs
887 = K-feldspar; Ab = albite; Ann = annite; Ptl = protolithionite

888

889 **Figure 4.** Huangshan granites geochemistry: a. ACNK vs ANK diagram; the most
890 aluminous 15HS02 (MP granite) and ZK03 (MA granite) samples are also the most
891 altered (see text). b. Upper crust normalized spidergram for both the MP and MA
892 granites, which appear to be indistinguishable in this diagram. Average spidergrams for
893 RMG types are given for comparison (from Linnen and Cuney 2005). Upper crust values
894 from Rudnick and Gao (2003), save for Li (Teng et al. 2004). PLK-RMG: peralkaline
895 rare metal granites and pegmatites; PLP-RMG: metaluminous to peraluminous, low-P
896 rare metal granites and pegmatites; IHP- and PHP-RMG: peraluminous intermediate and
897 high-P rare metal granites and pegmatites, including LCT-type [Li–Cs–Ta].

898

899 **Figure 5.** BSE images of accessory minerals in the micas from MP granite (a-d) and MA
900 granite (e-h). (a, b) Assemblage of zircon and a complex association of fluorite with Th-
901 rich bastnäsite, showing the transformation of primary Y-rich Fl-I + REE-fluoride into
902 REE-fluorocarbonate and Fl-II. (c) Symplectic association of Fluorite-I with fluocerite.
903 (d) Alteration of the Li-Fe mica into muscovite and Nb-rutile. (e) Partial replacement of
904 fluocerite by a La-rich bastnäsite; (f) A unique occurrence of Fl-I hosting small crystals of
905 U-pyrochlore) and columbite-(Fe). (g) Bastnäsite blades and thorite crystals included in a
906 chlorite matrix. (h) Nb-rutile and chlorite along the cleavages of altered annite. Fl =
907 fluorite; Th-rich Bast-(Ce) = Th-rich Bastnäsite- (Ce); Zrn = Zircon; Chl = Chlorite; Rt =
908 Rutile; Clb = Columbite-(Fe); U-Pcl = Uranian pyrochlore; Ms = Muscovite; Ptl =
909 Protolithionite; Ann = Annite

910

911 **Figure 6.** The Huangshan granite micas in (a) the Al (iv+vi)–R^{2+}–Si diagram of Monier
912 and Robert (1986), (b) the Li–R^{2+}–Al diagram of Foster (1960) and (c) the Fe + Mn + Ti–
913 Al^{VI} vs Mg–Li diagram of Tischendorff et al. (1997)

914

915 **Figure 7.** Nb content in the micas from Huangshan granites: (a), (c) MP and MA granites
916 histograms obtained by LA-ICP-MS, (b), (d) Nb averages and standard deviations from
917 SEM-EDS, EPMA and LA-ICP-MS data.

918

919 **Figure 8.** LA-ICP-MS data for the mica from the Huangshan MA and MP granites. (a)
920 Nb vs Nb/Ta, (b) Nb vs Ta, (c) Nb vs W, (d) Nb vs Sn, (e) Nb vs Li_2O, (f) Nb vs F, (g) Nb

vs FeO, (h) Nb vs Ti.

Figure 9. Comparison in a Ta–Nb diagram of the Huangshan micas (this work) with micas from rare-metal pegmatites and granites worldwide (Linnen and Cuney 2005 and references therein). Values for the upper continental crust, lower continental crust, N-MORB, and C-1 Chondrite are also shown. The detailed definition of PHP-, IHP-, PLP-, PLK-RMG, see the text.

This is a preprint, the final version is subject to change, of the American Mineralogist (MSA)
Cite as Authors (Year) Title. American Mineralogist, in press.
DOI: https://doi.org/10.2138/am-2018-6511

929 **Figure 1**

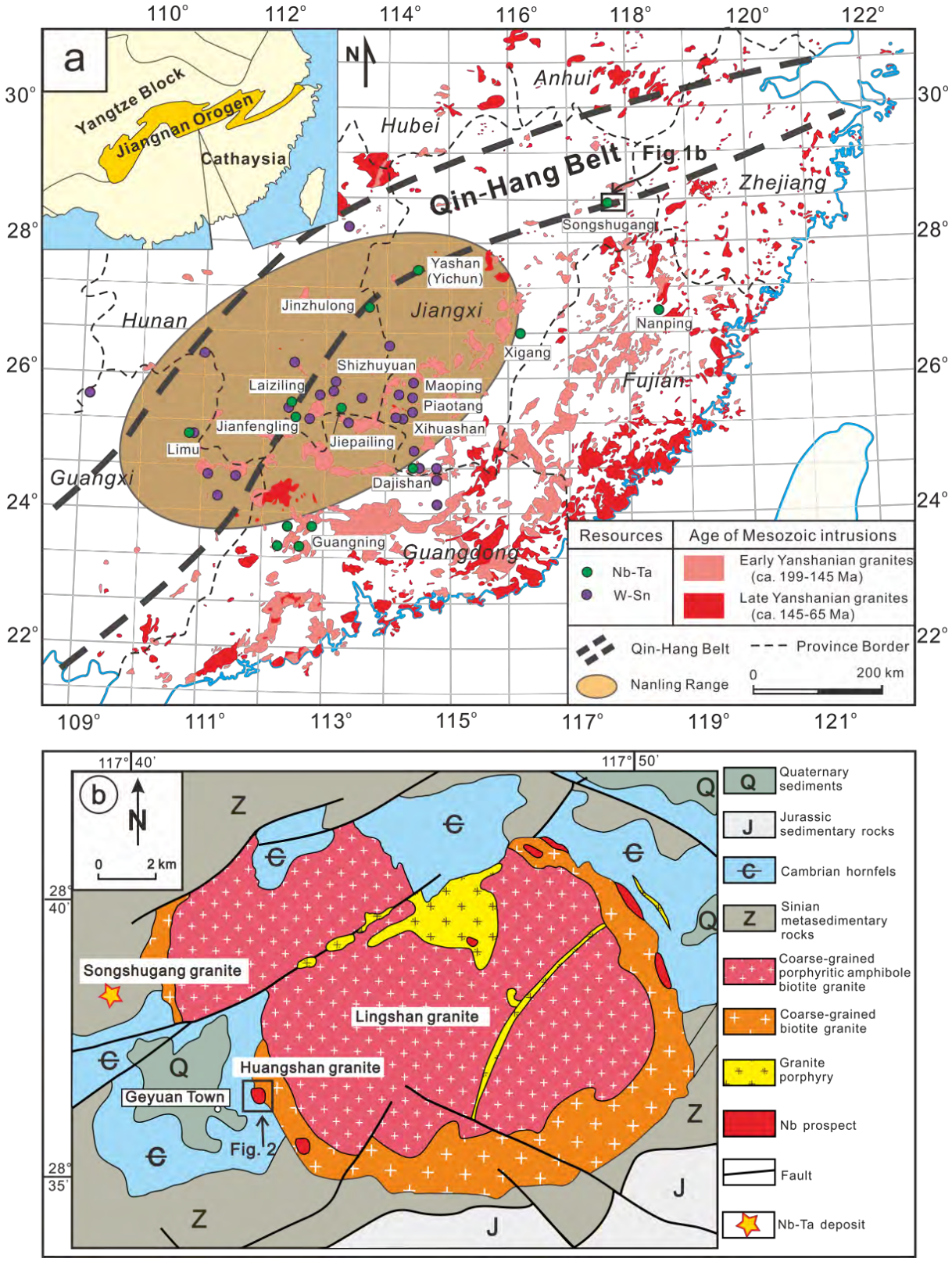

930

This is a preprint, the final version is subject to change, of the American Mineralogist (MSA)
Cite as Authors (Year) Title. American Mineralogist, in press.
DOI: https://doi.org/10.2138/am-2018-6511

931 **Figure 2**

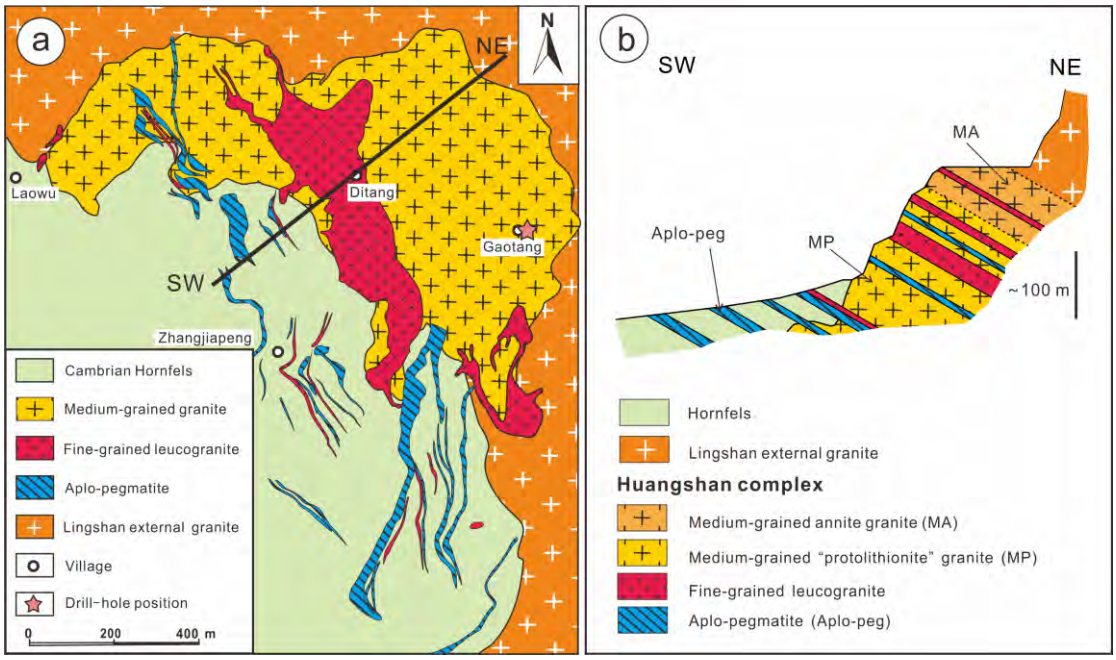

932

This is a preprint, the final version is subject to change, of the American Mineralogist (MSA)
Cite as Authors (Year) Title. American Mineralogist, in press.
DOI: https://doi.org/10.2138/am-2018-6511

933 **Figure 3**

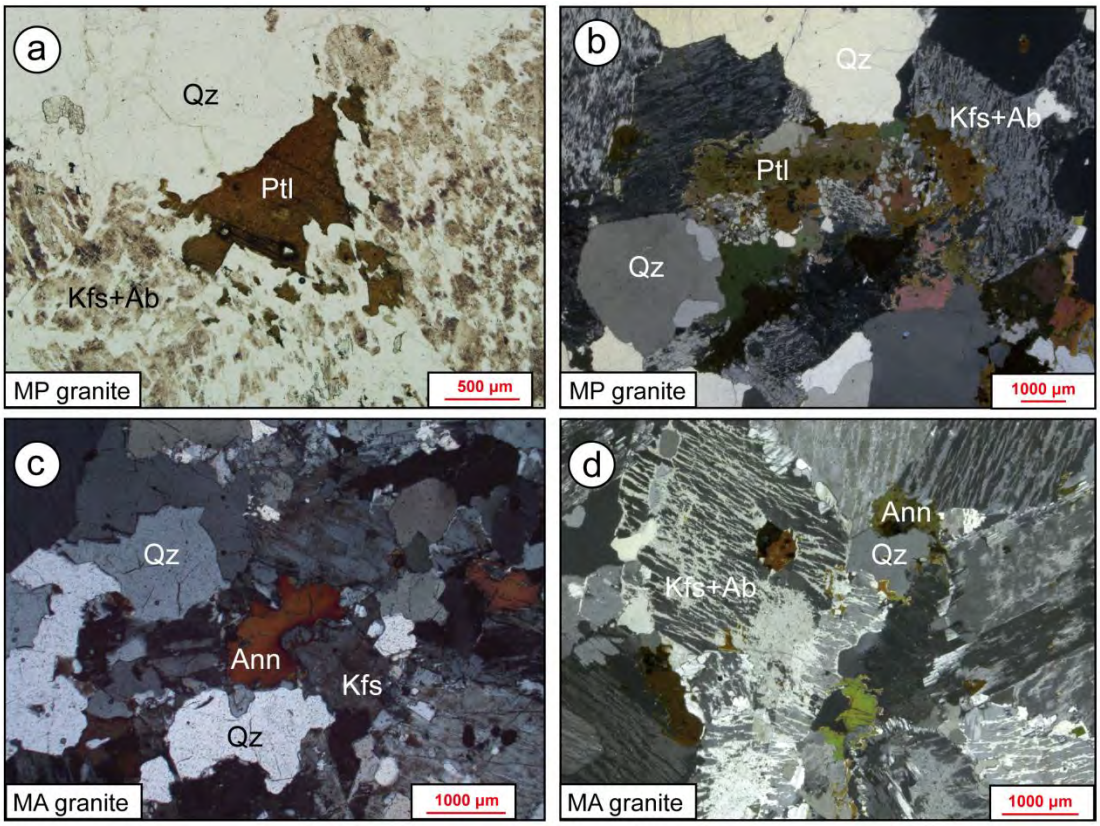

934

This is a preprint, the final version is subject to change, of the American Mineralogist (MSA)
Cite as Authors (Year) Title. American Mineralogist, in press.
DOI: https://doi.org/10.2138/am-2018-6511

935 **Figure 4**

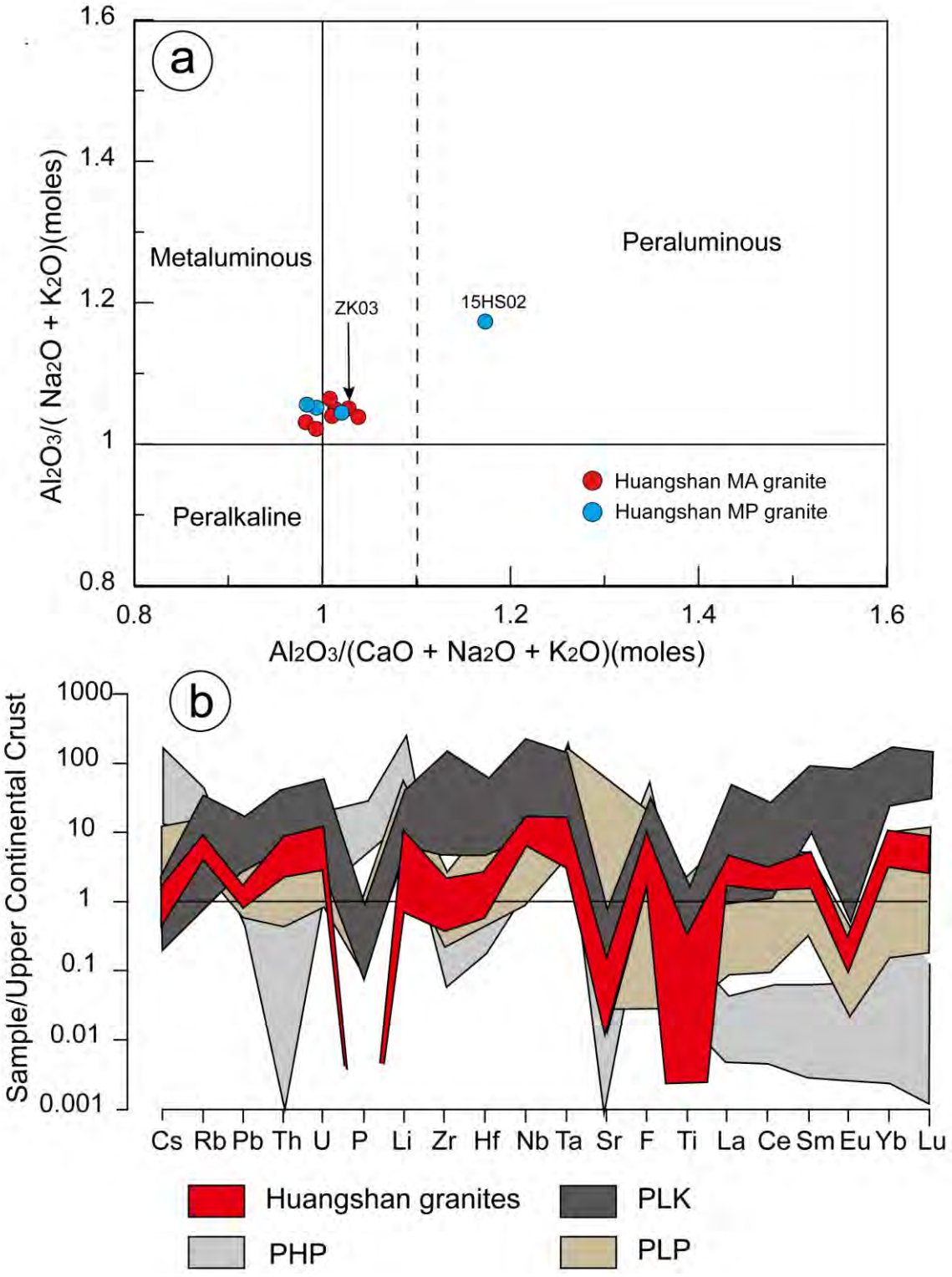

936

This is a preprint, the final version is subject to change, of the American Mineralogist (MSA)
Cite as Authors (Year) Title. American Mineralogist, in press.
DOI: https://doi.org/10.2138/am-2018-6511

937 **Figure 5**

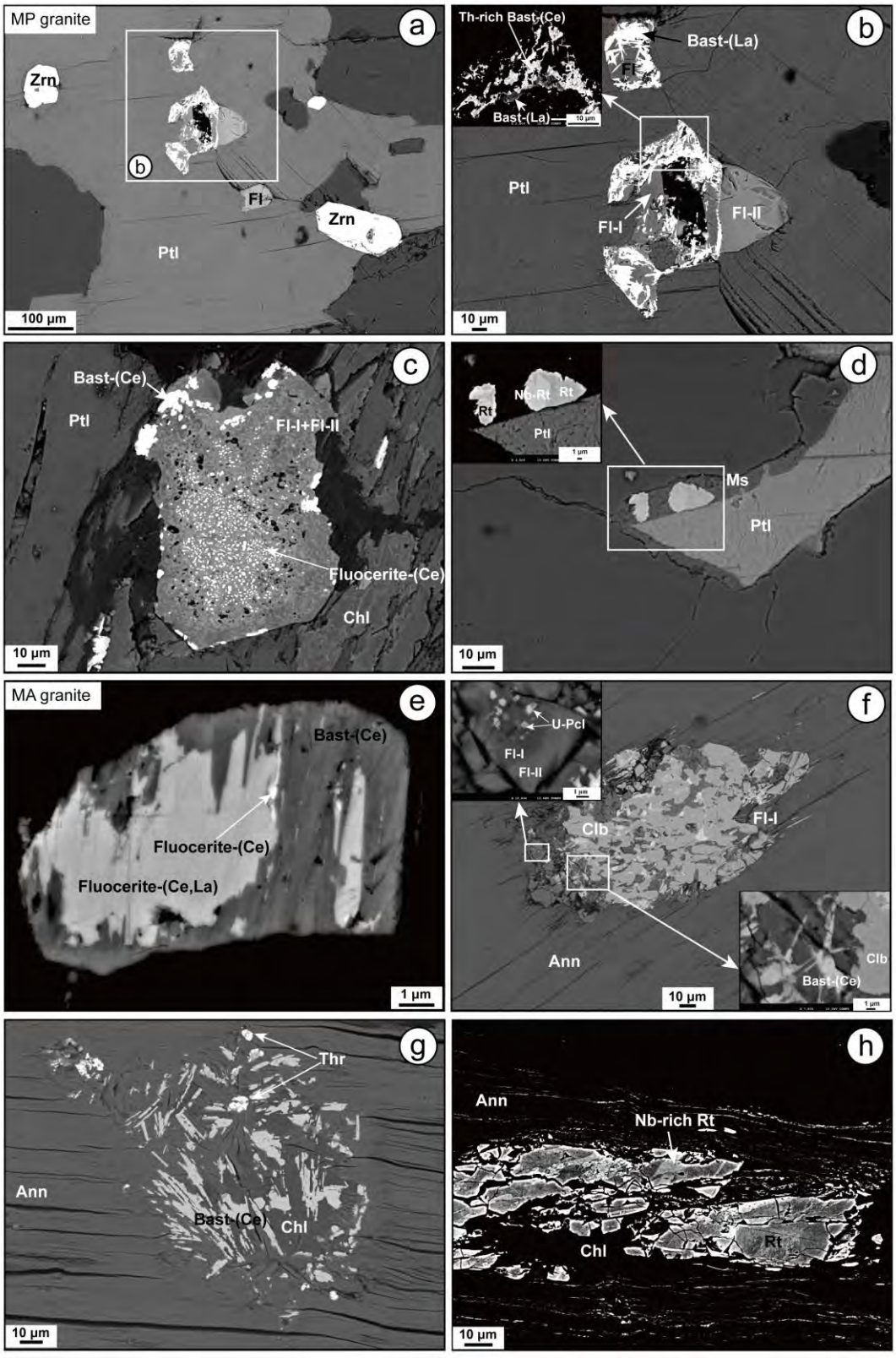

938

This is a preprint, the final version is subject to change, of the American Mineralogist (MSA)
Cite as Authors (Year) Title. American Mineralogist, in press.
DOI: https://doi.org/10.2138/am-2018-6511

939 **Figure 6**

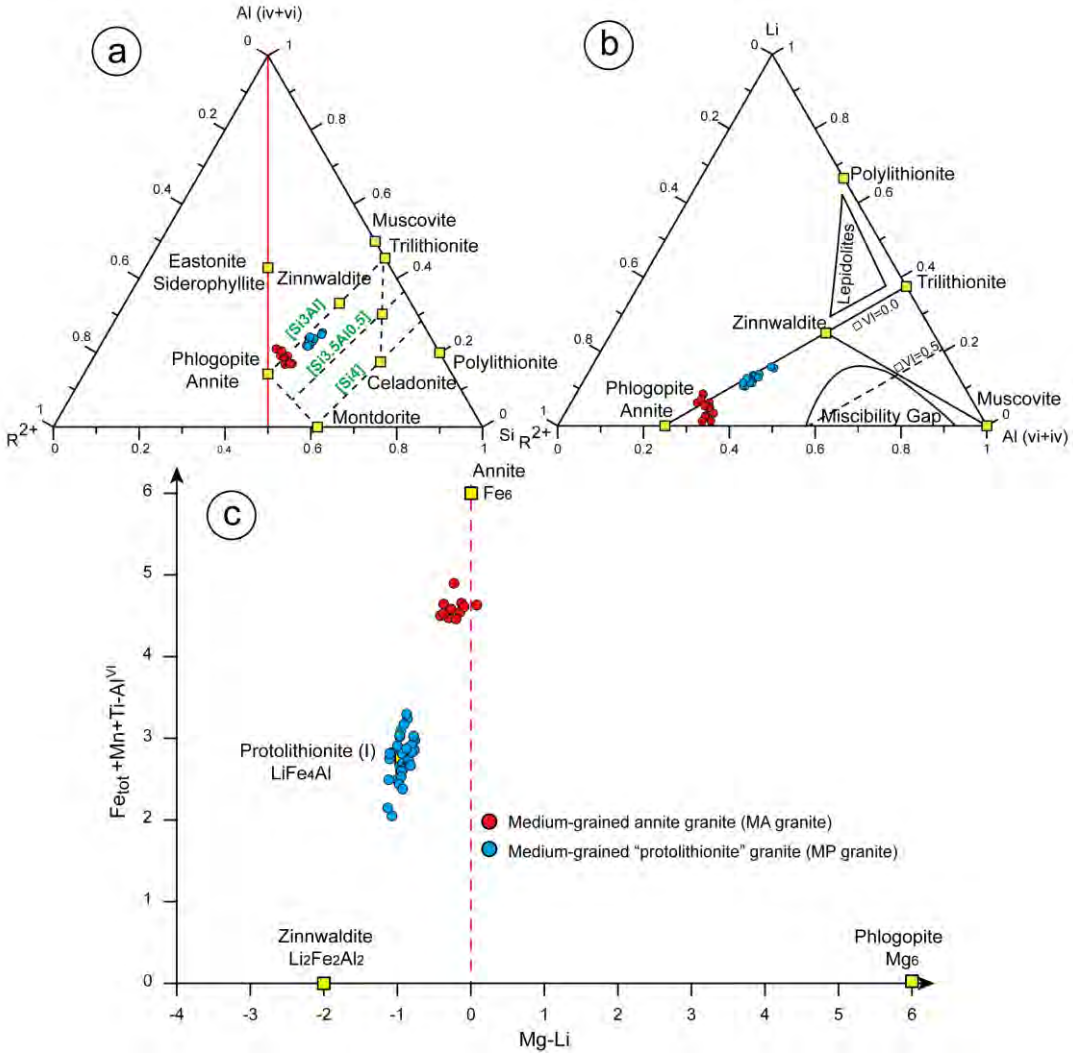

940

This is a preprint, the final version is subject to change, of the American Mineralogist (MSA)
Cite as Authors (Year) Title. American Mineralogist, in press.
DOI: https://doi.org/10.2138/am-2018-6511

941 **Figure 7**

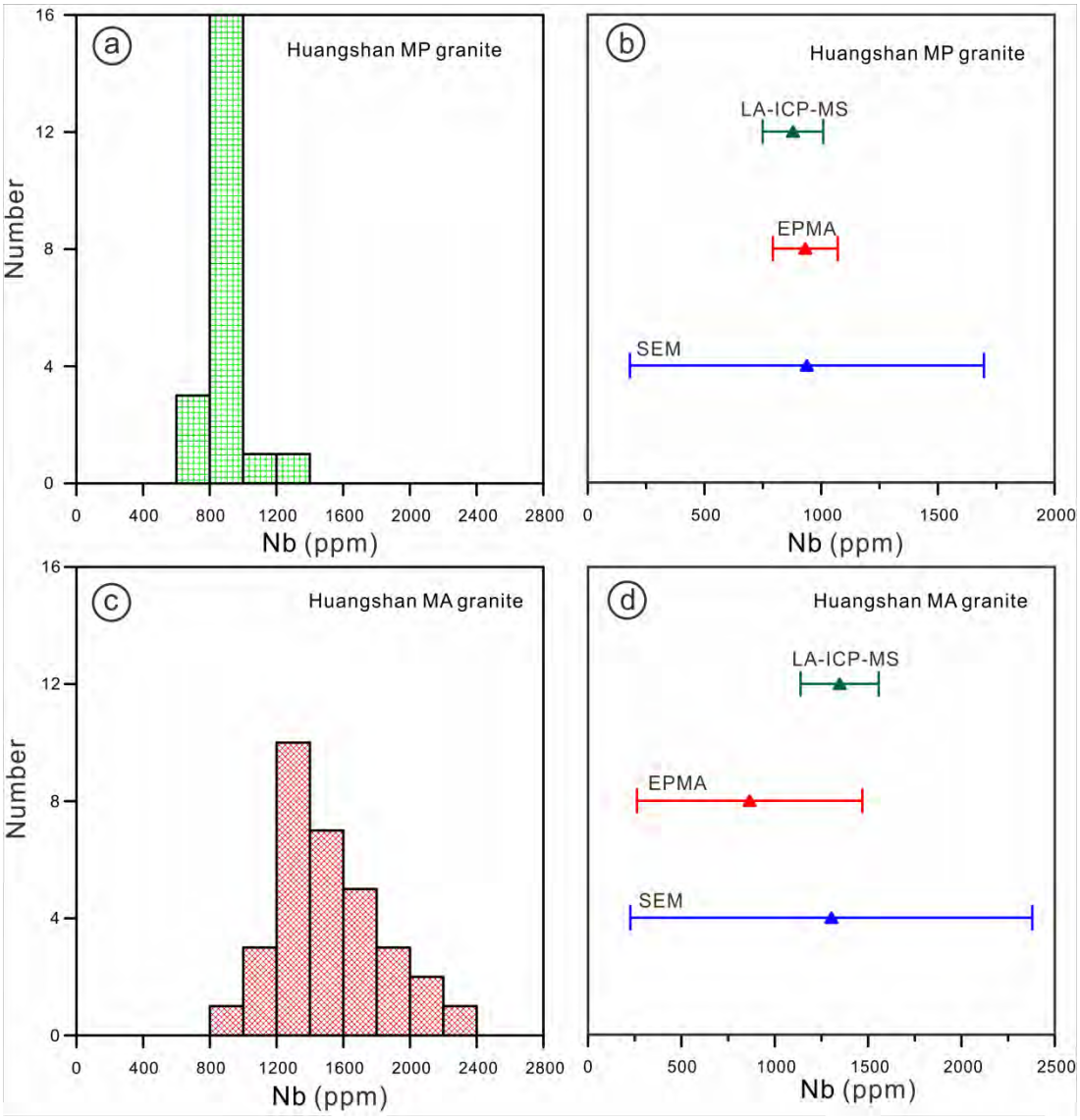

942

This is a preprint, the final version is subject to change, of the American Mineralogist (MSA)
Cite as Authors (Year) Title. American Mineralogist, in press.
DOI: https://doi.org/10.2138/am-2018-6511

943 **Figure 8**

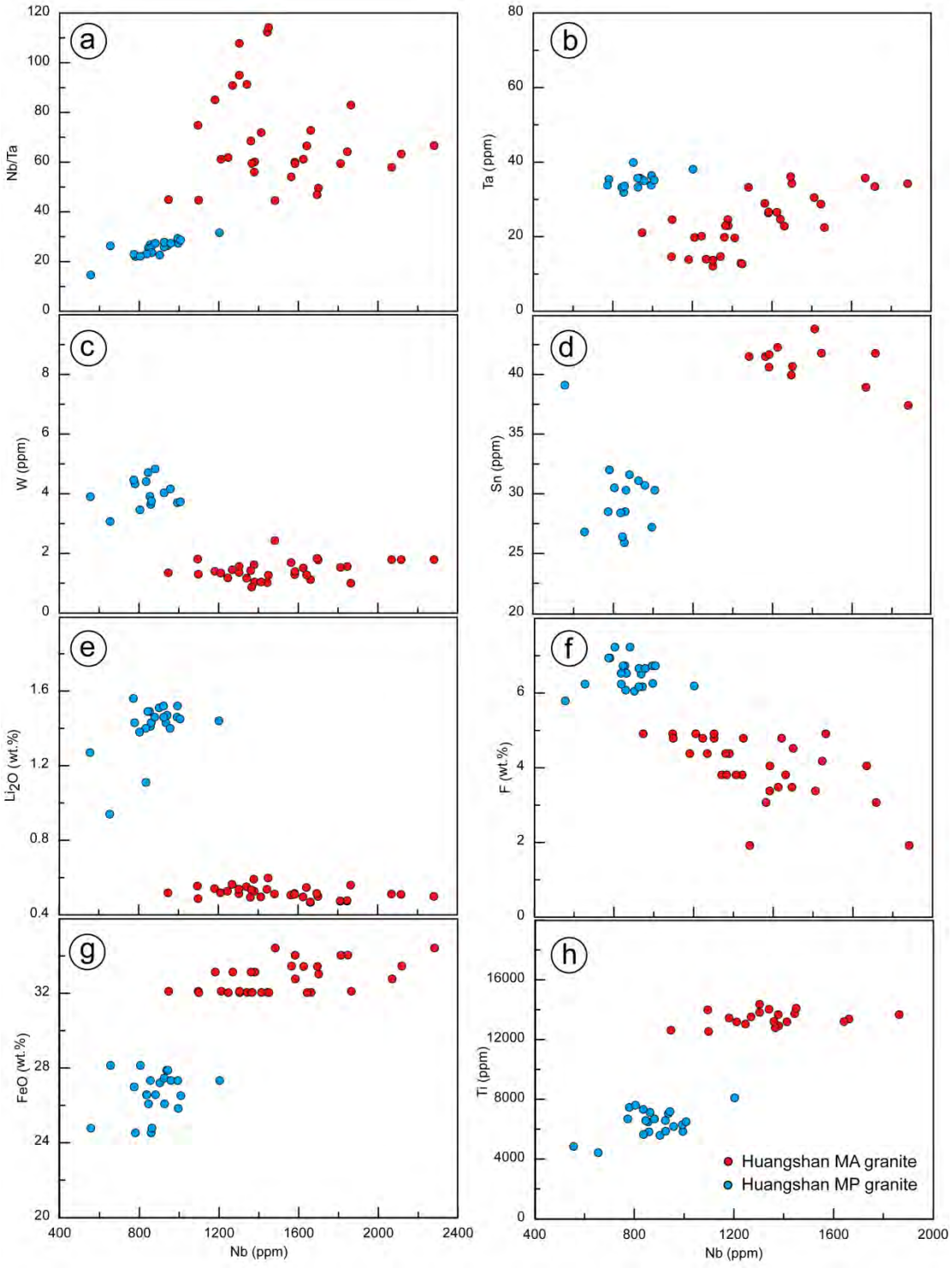

944

This is a preprint, the final version is subject to change, of the American Mineralogist (MSA)
Cite as Authors (Year) Title. American Mineralogist, in press.
DOI: https://doi.org/10.2138/am-2018-6511

945 **Figure 9**

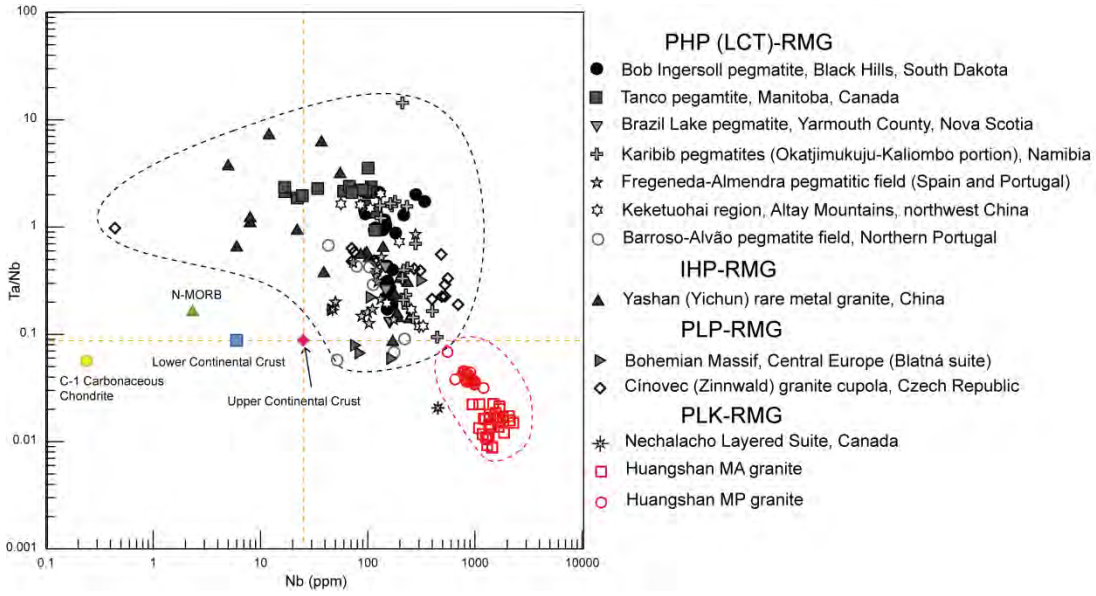

946

947

948 **Table 1 Major Nb-Ta-bearing minerals**

Mineral	Formula
Pyrochlore	$(Na,Ca)_2Nb_2O_6(OH,F)$
Columbite	$(Fe,Mn)(Nb,Ta)_2O_6$
Wodginite	$(Mn,Fe)\ (Sn,Ti)(Ta,Nb)_2O_8$
Ixiolite	$(Ta,Nb,Mn,Fe,Sn,Ti)_4O_8$
Microlite	$(Na,Ca)_2Ta_2O_6(O,OH,F)$
Nb-rich rutile	$(Ti,Nb,Ta,Fe,Sn)O_2$
Loparite	$(Na,REE,Ca,Sr,Th)(Ti,Nb,Ta)O_3$
Fergusonite	$REENbO_4$

949